MAST CELL REGULATION OF LARGE CHOLANGIOCYTE FUNCTION VIA H2 HISTAMINE RECEPTOR SIGNALING AND SUBSEQUENT LIVER DAMAGE

A Dissertation

by

LINDSEY LEANN KENNEDY

Submitted to the Office of Graduate and Professional Studies of
Texas A&M University
in partial fulfillment of the requirements for the degree of

DOCTOR OF PHILOSOPHY

Chair of Committee,	Gianfranco Alpini
Co-Chair of Committee,	Heather Francis
Committee Members,	Cynthia Meininger
	Fanyin Meng
Head of Department,	Warren Zimmer

May 2019

Major Subject: Medical Sciences

ABSTRACT

Histamine, synthesized by L-histidine decarboxylase (HDC), is a trophic growth factor that increases biliary damage/proliferation, inflammation, hepatic fibrosis and angiogenesis. Histamine signals through one of four G protein-coupled receptors, H1-H4 histamine receptors (HRs). Cholangiocytes, the epithelial cells that line the biliary tree of the liver, can be subdivided into small (~8 μm in size) and large (~15 μm in size) cholangiocytes, which have phenotypical and functional differences. H1HR is primarily found on small cholangiocytes, whereas H2HR is predominantly found on large cholangiocytes. Mast cells (MCs) (i) infiltrate the liver during cholestasis, (ii) reside near large ducts and (iii) release large amounts of histamine that mediates damage. We aimed to identify the role of MC-derived histamine on large cholangiocyte damage/proliferation via H2HR signaling, and subsequent liver injury in models of cholestasis.

We found that bile duct ligation (BDL, a model of cholestasis) induces large cholangiocyte damage, concomitant with increased MC infiltration near large ducts, and promotes liver inflammation, fibrosis and angiogenesis. MC-deficient mice subjected to BDL have reduced large cholangiocyte injury, mediated by decreased H2HR signaling, and reduced liver injury. Reintroduction of MCs into MC-deficient mice enhanced large cholangiocyte H2HR signaling, with an increase in large duct damage, as well as liver inflammation, fibrosis and angiogenesis. Multidrug resistance-2 knockout mice (*Mdr2*$^{-/-}$ mice, a model of primary sclerosing cholangitis) have increased large duct damage alongside increased H2HR signaling. Consequently, *Mdr2*$^{-/-}$ mice show increased liver inflammation, fibrosis and angiogenesis. Inhibition of large cholangiocyte H2HR signaling

by Vivo Morpholino treatment reduced these parameters. *In vitro*, MCs preferentially migrated towards damaged large, but not small, cholangiocytes. *In vitro,* large cholangiocytes treated with MC supernatants have increased damage and H2HR signaling, that is ameliorated when MCs are pre-treated with an HDC inhibitor (to block MC-derived histamine).

In conclusion, MC-derived histamine promotes large duct damage during cholestasis via H2HR signaling. Increased hepatic MC infiltration and large duct H2HR activation promotes liver inflammation, fibrosis and angiogenesis. Inhibition of MC activation or large duct H2HR signaling reduces these damaging effects. Blocking MCs or large cholangiocyte H2HR activity may be a therapeutic option for patients suffering from large duct damage.

DEDICATION

This dissertation is dedicated to my family: Mom, Dad, Megan, Allison and Garrett. Your understanding, support and encouragement during moments of difficulty helped to remind me that I was on the right path.

'There's nowhere you can be that isn't where you're meant to be'

All You Need Is Love by the Beatles

A song I fondly remember singing in the car during long family trips.

ACKNOWLEDGEMENTS

Following 3.5 years of work, I am honored to have finally reached the moment where I can write this dissertation. This milestone would not have been attainable without the help and support of many people. While the title page states that this is *A Dissertation by Lindsey Leann Kennedy* it is truly a dissertation that consists of multiple "co-authors" that I would like to acknowledge here.

I would like to thank my committee members, Dr. Meininger and Dr. Meng for their insightful comments throughout this research.

I would like to thank all of the members of the Digestive Diseases Research Center who supported this dissertation. Special thanks go to all members of the Francis lab, both past and present. Specifically, I would like to thank Laura Hargrove, Jennifer Demieville and Vik Meadows for helping with experiments and for their friendship.

This dissertation would not have been developed without the strong support and guidance from Dr. Heather Francis and Dr. Gianfranco Alpini, who served as the yin and yang in my scientific career (even though it was more yin and yin at times). Your patience and leadership were undeniably valuable for the completion of this dissertation and will help me throughout my scientific career.

Finally, I would like to acknowledge my family who provided constant encouragement, as well as a sympathetic ear throughout my graduate school experience. My close friends and family acted as my biggest fans and provided continuous support, which I will forever be grateful for.

CONTRIBUTORS AND FUNDING SOURCES

Contributors

This work was supported by a dissertation committee consisting of Drs. Gianfranco Alpini (chair), Heather Francis (co-chair), Cynthia Meininger (committee member), and Fanyin Meng (committee member). Drs. Heather Francis and Gianfranco Alpini are in the Department of Medical Physiology at Texas A&M Health Science Center and the Central Texas Veterans Healthcare System. Dr. Cynthia Meininger is in the Department of Medical Physiology at Texas A&M Health Science Center. Dr. Fanyin Meng is in Academic Operations at Baylor Scott & White Health and the Central Texas Veterans Healthcare System.

Pathological analysis of H&E staining was performed by Dr. John Greene, Jr., a certified pathologist at Baylor Scott & White Health during the time of analysis. All other work conducted for the dissertation was completed by the student independently.

Portions of this work were previously published in *Hepatology* in the following publication: 'Hargrove L, Kennedy L, Demieville J, Jones H, Meng F, DeMorrow S, Karstens W, Madeka T, Greene J Jr, Francis H. *Hepatology*. 2017 Jun;65(6): 1991-2004.'

Funding Sources

This work was supported by VA Merit Awards and NIH NIDDK R01 grants. The authors have no financial conflicts and the views expressed in this dissertation are those of the author(s) and do not necessarily represent the views of the Department of Veterans Affairs.

NOMENCLATURE

αMe	α-methyl-dl-histidine
Ang-1	Angiopoietin-1
BDL	Bile duct ligation
cAMP	Cyclic adenosine monophosphate
CCA	Cholangiocarcinoma
CK-19	Cytokeratin-19
CCl_4	Carbon tetrachloride
EIA	Enzyme immunoassay
ELISA	Enzyme-linked immunosorbent assay
FGF	Fibroblast growth factor
FN-1	Fibronectin-1
HDC	L-histidine decarboxylase
HR	Histamine receptor
HSC	Hepatic stellate cell
IBDM	Intrahepatic bile duct mass
IL	Interleukin
LPS	Lipopolysaccharide
MC	Mast cell
Mdr2$^{-/-}$	Multidrug resistance 2 knockout
mMCP-1	Mouse mast cell protease-1
NGF	Neural growth factor

PAI-1	Plasminogen activator inhibitor type 1
PBC	Primary biliary cholangitis
pERK	Phosphorylated p44/42 mitogen-activated protein kinases
PSC	Primary sclerosing cholangitis
*q*PCR	Quantitative real-time polymerase chain reaction
SCF	Stem cell factor
SEM	Standard error of the mean
SYP-9	Synaptophysin-9
TGF-β1	Transforming growth factor-β1
TNF-α	Tumor necrosis factor-α
VEGF	Vascular endothelial growth factor
vWF	von Willebrand factor

TABLE OF CONTENTS

LIST OF FIGURES

CHAPTER I

INTRODUCTION AND LITERATURE REVIEW

The Liver and Hepatic Cell Types

The liver is a complex organ that regulates key functions necessary for maintaining cellular homeostasis. The liver plays important roles in detoxification, drug metabolism, lipid metabolism and bile acid synthesis/secretion (1). The liver is comprised of multiple cell types including hepatocytes, Kupffer cells (resident macrophages), hepatic stellate cells (HSCs), liver sinusoidal endothelial cells, biliary epithelial cells (cholangiocytes), and other resident and infiltrating cell types (1).

Cholangiocytes

Cholangiocytes are the epithelial cells that line the intrahepatic and extrahepatic ducts of the biliary tree and are the target of cholangiopathies, such as primary sclerosing cholangitis (PSC), primary biliary cholangitis (PBC) and cholangiocarcinoma (CCA). Cholangiocytes make up ~3-5% of the hepatic cell population, so while this cell type does not make up the majority of the liver, we and others have shown that cholangiocytes have key roles in the maintenance of hepatic homeostasis under normal conditions, and the promotion of disease progression following injury (2-4). Cholangiocytes are primarily known for their modification of bile composition and detoxification of xenobiotics, and during normal conditions they are mitotically dormant (5). During biliary-specific damage (i.e. cholangiopathies) cholangiocytes begin to proliferate and secrete a number of neuroendocrine factors that influence the surrounding microenvironment (2, 4, 5). In particular, biliary-derived vascular endothelial growth factor (VEGF)-A/C acts as a growth

promoting factor for the endothelial cells of the peribiliary vascular plexus (6). Similarly, other factors secreted from cholangiocytes, such as histamine, serotonin, substance P and neural growth factor (NGF) can act in both autocrine and paracrine manners to promote disease progression during cholestasis (7-12).

Cholangiocytes are heterogenous and can be subcategorized as either small (<15 μm diameter, line the small bile ducts) or large (≥15 μm diameter, line the large bile ducts) cholangiocytes in rodents (2, 4). Not only do small and large cholangiocytes vary in size, but they vary in function and response to damage (3, 13, 14). It has been reported that large cholangiocytes are more susceptible to damage and become senescent, which has been hypothesized to promote disease progression during cholangiopathies (10-12, 15). Functionally, small cholangiocytes promote their proliferation through Ca^{2+}-dependent mechanisms, whereas large cholangiocytes increase their proliferation via cyclic adenosine monophosphate (cAMP)/phosphorylated p44/42 mitogen-activated protein kinases (pERK) signaling (2, 7, 13, 15, 16). Further, we have demonstrated that small cholangiocytes express the H1 histamine receptor (H1HR), whereas large cholangiocytes express H2HR (7). It is interesting to note that Ca^{2+} signaling is downstream of H1HR, whereas H2HR activation leads to cAMP/pERK signaling, which mimics the functional signaling mechanisms that are known to promote small versus large cholangiocyte proliferation (2, 4, 7, 13, 16). Further, multidrug resistance-2 knockout (*Mdr2*$^{-/-}$, a model of PSC) mice show a slight increase in H1HR expression primarily in small (minimally in large) cholangiocytes, but a significant increase in H2HR in large (but not small) cholangiocytes (15). Similarly, human PSC patients show increased biliary H1HR and H2HR expression; however, the expression of these HRs in human small versus large

ducts has not been demonstrated (15). PBC is characterized by ductopenia of the small ducts; therefore, one could assume that H1HR signaling may play a role in PBC progression. However, ~70% of PSC cases are characterized by large duct damage, which eludes to the role of H2HR signaling in this disease. In support of this, we have found that, in *Mdr2*$^{-/-}$ mice, where we see an increase in large H2HR expression, we subsequently see an increase in predominantly large duct mass (15). Therefore, we hypothesize that increased large duct H2HR expression and signaling promotes the progression of PSC.

Proliferation of large ducts has been hypothesized to be supported by a stem cell niche found within the peribiliary glands (17, 18). The peribiliary glands contain serous and mucinous acini, as well as stem/progenitor cells, and reside near large ducts (17-19). The peribiliary glands are structurally and mechanistically different from hepatic progenitor cells, which are the stem/progenitor cell population that reside near and repopulate the small cholangiocyte population during specific injury (19). It has been demonstrated that the peribiliary glands become activated during cholestatic injury, including PSC, and may increase the proliferation of the stem/progenitor cells, as well as their differentiation into large cholangiocytes (17, 18).

Kupffer Cells

Kupffer cells are the tissue-resident macrophages in the liver that contain phagocytic capabilities but can mediate hepatic inflammation as well (20, 21). Kupffer cells, like other macrophages, maintain innate immunity within the liver through the phagocytosis of infectious materials and cellular debris (20). Kupffer cells reside within the sinusoids of the liver and have immediate surveillance of pathogens entering via the

portal venous system (22). Additionally, Kupffer cells can be activated by various factors to induce a strong inflammatory response (21). Activated Kupffer cells respond to, and secrete, various cytokines and chemokines that drive hepatic inflammation, especially in the setting of cholestasis (21, 23). During a pro-inflammatory state, Kupffer cells can release tumor necrosis factor (TNF)-α, interleukin (IL)-6, IL-1β and transforming growth factor (TGF)-β1 that promote liver damage (24, 25). Secretion of these and other factors from Kupffer cells allows paracrine interactions with nearby cells to mediate their response. For instance, Kupffer cells can communicate with HSCs (also located in the hepatic sinusoids) during liver injury to induce HSC activation (26, 27). Kupffer cells also signal to hepatocytes to influence disease progression following liver damage (28, 29); however, signaling between Kupffer cells and cholangiocytes has yet to be elucidated. Furthermore, Kupffer cells can influence the infiltration of other cells, such as neutrophils (30), so they may have an unknown impact on MC migration and activation.

Hepatic Stellate Cells (HSCs)

Hepatic fibrosis is characterized by the accumulation of extracellular matrix (ECM) and is the byproduct of chronic liver injury including cholestasis (31). ECM deposition during liver injury is mediated by myofibroblasts, which can arise from activated HSCs or portal fibroblasts, but HSC activation contributes to collagen deposition and liver fibrosis to a greater degree than activated portal fibroblasts (32). In a normal state, HSCs are quiescent and store vitamin A, but following injury they transdifferentiate into myofibroblasts that contain contractile, inflammatory and fibrogenic properties (33). The initiation of HSCs is defined by the activation of this cell type by specific factors, secreted from nearby cells, causing HSCs to increase their expression of growth factor receptors

and fibrogenic response. Perpetuation of these events amplifies activated HSC phenotypes, thus pushing them to a myofibroblast state (34). TGF-β1 is one of the most potent activators of HSCs (35), and HSC activation can be mediated by various cell types, including cholangiocytes (11, 12). Specifically, cholangiocyte-derived TGF-β1 and senescence-associated secretory phenotypes (SASPs) have been shown to promote HSC activation and liver fibrosis during models of cholestasis (11, 12). There is a correlation between increased MC infiltration and HSC activation/fibrogenesis exhibited in models of cholestasis (15, 36, 37); therefore, infiltrating and activated MCs may play a role in HSC activation and ECM remodeling.

Endothelial Cells

The liver has its own well-defined vasculature that is crucial for development, tissue growth and regeneration (38). Angiogenesis is the formation of new vessels from the existing vasculature and can occur within the liver during growth and repair (39). Angiogenesis has a key role in physiology, but can influence pathology as well. In particular, angiogenesis has been shown to contribute to inflammatory and fibrogenic responses during chronic liver disease (40-42). During chronic liver injury, persistent inflammation causes increased vascular permeability and promotes the recruitment of immune and inflammatory cells (43, 44), which may include MCs. In turn, these infiltrating cells can secrete cytokines and growth factors that further promote endothelial cell proliferation and migration (45, 46). During the angiogenic process, ECM remodeling is necessary for new sprout formation (47, 48). ECM remodeling is also a key process for the progression of liver fibrosis, indicating that these two activities are closely intertwined. Several angiogenic factors, including VEGF, fibroblast growth factor (FGF) and

angiopoietin (Ang)-1 induce endothelial cell proliferation and tube formation, thereby promoting angiogenesis (49, 50), and these factors can be derived from cholangiocytes, as well as from MCs (6, 51, 52). The biliary tree has its own vascular network termed the peribiliary vascular plexus, which resides in close proximity to large bile ducts (53). It has been nicely demonstrated that the blood supply from the peribiliary vascular plexus nourishes the biliary tree during growth, but in turn growth factors secreted by cholangiocytes support the peribiliary vascular plexus (6, 54). In addition, Kupffer cells and HSCs may play a prominent role in angiogenesis during injury (55, 56). It is evident that there are complex signaling mechanisms and cellular interactions that occur during the progression of liver disease to influence biliary damage, inflammation, liver fibrosis and angiogenesis.

Human Cholestatic Liver Diseases

Cholestasis is generally characterized by the impairment of bile flow, causing accumulation of toxic bile acids in the liver (57, 58). Normal bile physiology is dependent on various membrane transporters and nuclear receptors found on hepatocytes as well as cholangiocytes (59, 60). Mutations in various bile acid transporters has been linked to increased susceptibility of developing various cholestatic diseases; specifically, *MDR3* mutations have been linked to PSC, *ABCB11* mutations in progressive familial intrahepatic cholestasis, and more recently *SLC51B* mutations in the development of congenital diarrhea coupled with cholestasis (61, 62). However, there may be other factors mediating disease onset and progression, such as infection, gut dysbiosis, improper immune response and environmental factors (63, 64).

Cholestatic diseases targeting the cholangiocytes (i.e. cholangiopathies) are progressive diseases leading to end-stage liver disease with few to no therapeutic options (64, 65). PBC and PSC are two of the main cholangiopathies, accounting for approximately two-thirds of patients referred for liver transplantation (66). In fact, approximately 16% of liver transplants performed in the United States between 1988 and 2014 were for cholangiopathies (63). It is apparent that the treatment of cholangiopathies remains a significant problem; therefore, understanding mechanisms of disease progression may lead to better therapeutics for patients.

Primary Biliary Cholangitis

PBC is a chronic, cholestatic liver disease characterized by inflammation, bridging fibrosis and ductopenia at later stages, and may progress to cirrhosis during end-stage disease (63, 67). The prevalence of PBC is approximately 40 per 100,000 people, but these rates have gradually risen over time, according to a 2012 study (68). It is interesting to note that approximately 90% of PBC patients are female, with the average age of diagnosis being 55 years (69). Patients are diagnosed with PBC by having more than twice the upper limit of normal alkaline phosphatase (ALP) serum levels, alongside positive serum antimitochondrial antibodies (70). Ursodeoxycholic acid (UDCA) was the first FDA-approved therapy for the treatment of PBC, but 30-40% of patients fail to respond to this treatment (67). Obeticholic acid (OCA) was the second FDA-approved treatment for PBC, specifically for patients that were unresponsive or intolerant to UDCA, but only around 50% of patients showed significant reductions in serum ALP following OCA treatment (67, 71). As well, long-term outcomes of OCA treatment, such as rates for liver transplantation and mortality, are unknown (67, 71). While PBC is considered an

autoimmune disease, patients do not respond to typical immunosuppressive agents, making the treatment for this disease even more complicated (72).

Primary Sclerosing Cholangitis

PSC is characterized by chronic, peribiliary inflammation and fibrosis that can lead to stricturing of the ducts (obstructive cholestasis), and eventual cirrhosis and end-stage disease (63, 73). The prevalence of PSC varies greatly, from 0 – 16.2 per 100,000 people, but similar to PBC the prevalence of PSC is on the rise (68). PSC is primarily diagnosed in males, with the average age of diagnosis being 30 – 40 years (73). Of interest, approximately 70% of patients diagnosed with PSC also present with some form of inflammatory bowel disease, typically ulcerative colitis, further underlining the inflammatory component of this disease (74). PSC is diagnosed by having serum ALP levels twice the upper limit of normal, cholangiographic evidence of biliary stricturing and the exclusion of secondary sclerosing cholangitis (73, 74). The majority of PSC cases are found to affect only the large ducts of the biliary tree, but there is a small portion of PSC cases that show damage to the small ducts (75), and it is currently unknown why certain portions of the biliary tree are affected in different cases. It is also important to note that CCA is found in conjunction with PSC in 20 – 30% of diagnoses, and in 50% of cases 1 year after diagnosis (76). Currently, there are no effective therapies for the treatment of PSC, with liver transplantation being the only treatment option (63); however, recurrence of PSC occurs in 25% of patients following transplantation (77).

Mast Cells

MCs were first characterized by Dr. Paul Ehrlich in 1878 (78). MCs are an immune cell type largely known for their mediation of allergies and inflammation; however, their role in autoimmune, infectious and other disorders is becoming more known (78-82). MCs originate from CD34+ hematopoietic stem cells following stimulation with stem cell factor (SCF) and ILs, which mediate the development of different MC subtypes (82). Upon leaving the bone marrow, MCs circulate throughout the body via the lymphatic and vascular systems and migrate towards damaged tissues where they complete their development, which is determined by the local microenvironment (83). MCs can be found throughout the body but are preferentially located in connective tissue and in mucosal sites (78-80). MC distribution and final location is dependent on constitutive homing, factors initiating recruitment, MC survival and local maturation (84, 85).

As stated, MCs finish their maturation once they reach their final destination; therefore, their receptor expression and secretion of factors vary greatly depending on the microenvironment (78, 79, 84). In humans, MCs are categorized based on their protease expression: MC_T for tryptase, and MC_{TC} for tryptase and chymase (86, 87). MC_T are generally found in mucosal sites, while MC_{TC} are mostly found in connective tissues (88, 89). Similarly, in rodents, the MC subpopulations are divided into connective tissue-type MCs (CTMCs) and mucosal-type MCs (MMCs) (88, 90). These two rodent populations can be distinguished by their specific markers; mast cell protease 1 (MCP-1) is found in CTMCs, while MCP-2 is found in MMCs (88, 91). In both humans and rodents, these different populations of MCs show different modes of activation and release of different molecules (92, 93), further cementing the concept of MC heterogeneity.

MCs express a plethora of surface markers, including FCεRI, complement receptors, HRs, toll-like receptors and serotonin receptors, which allows MCs to become activated by a number of factors (85). There are typical MC agonists that are known to promote MC migration; including, SCF, IgE, sphingosine-1-phosphate, histamine and various ILs and chemokines (15, 37, 88, 94); however, there are a number of non-traditional chemoattractants that have been identified. Leptin has been found to stimulate MC migration and pro-inflammatory activation (95), which may have implications for non-alcoholic fatty liver disease (NAFLD) and non-alcoholic steatohepatitis (NASH). Additionally, plasminogen activator inhibitor type 1 (PAI-1) secreted from keratinocytes recruits MCs to the skin, which in turn promotes fibrogenesis (96). Considering that PAI-1 is a senescence factor, and cholangiocytes become senescent during chronic liver injury, there may be a role of PAI-1 and other senescence factors for the migration and activation of MCs.

Following migration and activation, MCs increase cytokine production and degranulate to release a variety of substances, including histamine, proteases, serotonin, TGF-β1 and VEGF (79). Specifically, MC release of IL-17A following activation results in increased tissue inflammation in the skin and gut (97). Interestingly, it has been shown that activated MCs release microvesicles that can promote endothelial cell cytokine expression *in vitro* (98). As well, hepatitis C virus infection upregulates MC microRNA (miR)-490 expression and exosomal secretion, which can be taken up by hepatocytes *in vitro* (99). Work from our group has demonstrated that inhibition of MC-derived histamine reduces cholestatic liver injury, including biliary damage, liver fibrosis, angiogenesis, bile flow and total bile acid levels (100). Additionally, we have found that inhibition of MC-

derived TGF-β1 or farnesoid X receptor (FXR, nuclear receptor involved in bile acid synthesis) blocks cholestasis-induced liver injury (Kennedy, Meadows and Francis, unpublished observations, 2018).

Within the liver, MCs are primarily found near hepatic arteries, veins and bile ducts (37, 100). In normal livers, MCs are found in small number in portal areas, but MC number increases following injury (100-102). Our data indicates that damaged cholangiocytes, but not hepatocytes or HSCs, release factors that promote MC infiltration and activation (Kennedy and Francis, unpublished observations, 2017). In particular, we have previously shown that during CCA (i.e. cancer of the bile ducts) there is increased secretion of SCF that promotes MC migration via interaction with the receptor c-Kit (94). As well, increased hepatic MC number has been noted in PBC and PSC patients (100, 103), and similar to CCA, patients with PSC have increased c-Kit-positive MC infiltration near bile ducts expressing increased SCF (102). Furthermore, it has been demonstrated that MC presence correlates with increased stage of fibrosis in NASH (104); therefore, inhibition of MC migration or activation may be a therapeutic option for a number of diseases.

Specifically, we have shown that human CCA has increased MC infiltration, which is mediated by CCA-derived SCF binding to c-Kit on MCs (94). In rats subjected to bile duct ligation (BDL, a model of obstructive cholestasis), we note an increase in MC number, specifically in peribiliary areas, which increases over time and correlates with increased damage (37); an increase in MC number has also been shown in *Mdr2*$^{-/-}$ mice along with enhanced liver damage (100). However, treatment with cromolyn sodium (which inhibits MC degranulation and histamine release) in either BDL rats or *Mdr2*$^{-/-}$ mice reduces MC activation and subsequent liver damage (37, 100). Others have found that

MC-derived extracellular vesicles can be taken up by HSCs to promote their activation (105), further supporting the pro-fibrogenic role of MCs. Additionally, in the cholestatic model of carbon tetrachloride (CCl_4) treatment, there was an accumulation of hepatic MCs that correlated with increased steatosis and inflammation, which was blocked by vitamin E treatment (106). These studies elude to the therapeutic potential of blocking MC migration or activation during various liver injuries.

Models of Cholestasis

During normal conditions, cholangiocytes are mitotically dormant; however, during cholestatic injury cholangiocytes become hyperplastic, express a neuroendocrine phenotype and subsequently release factors that can promote MC activation, as well as damage to nearby hepatic cells (12, 15, 107, 108). Particularly, we know that injured cholangiocytes secrete histamine, VEGF, substance P, and senescence factors that may be involved in MC chemoattraction (9, 11, 51, 109). One of the classic models of cholestasis is the BDL model of obstructive cholestasis. With this model, the common bile duct is ligated, to block bile flow and mimic obstructive cholestasis and induce a strong inflammatory and fibrogenic reaction, alongside biliary injury (8, 16, 109). BDL is an established model that we regularly use in our lab (2, 8, 16, 109, 110), and we have previously demonstrated that following BDL, cholangiocytes become hyperplastic and hepatic MC migration/activation is significantly increased, thereby promoting liver damage (36, 101). Since BDL induces biliary damage reminiscent of cholestatic injury, and promotes the migration and activation of MCs, this model is beneficial for the studies of MCs during cholestatic liver injury.

Another commonly used model of cholestasis is the *Mdr2*$^{-/-}$ mouse model of PSC (111). These mice are lacking the ATP-binding cassette, sub-family B, member 4 (i.e. *Mdr2*), so they are unable to secrete phospholipids into the bile, thus leading to liver injury, sclerosing cholangitis and cholelithiasis (112). Specifically, this model mimics some characteristics similar to human PSC; such as increased biliary proliferation, inflammation, and peribiliary fibrosis, and these phenotypes further increase over time (15, 111). Since PSC patients show similar liver phenotypes, and since there is evidence for mutation of the *MDR3* gene (human ortholog of *Mdr2*), this model is ideal for the study of PSC (112). We have demonstrated that *Mdr2*$^{-/-}$ mice have increased MC number (15, 100), which increases over time and corresponds with increased disease progression (Kennedy and Francis, unpublished observations, 2018). Similar to the BDL model, the *Mdr2*$^{-/-}$ mouse is a useful tool for the study of cholestatic liver injury, specifically PSC, and MC promotion of this disease.

Histamine Signaling

Histamine is a biogenic amine that was first isolated and characterized in 1910 by Sir Henry Dale, who found that it had a stimulating effect on smooth muscle from the gut and the respiratory tract (113). Since then, histamine has largely been recognized for its modulation of inflammatory and allergic responses (114); however, the role of histamine in pathological responses is becoming more recognized.

Histamine is synthesized from the amino acid histidine by the enzyme L-histidine decarboxylase (HDC) (115, 116). Histamine synthesis increases in growing tissues (117); as well, studies have shown that HDC expression is increased in neuroendocrine tumors

and multiple malignant cell lines (15, 115, 118). Additionally, in adult animals the liver contains one of the highest concentrations of HDC (119). We have found that cholangiocytes have the highest expression of HDC and secretion of histamine when compared to other liver cell types, and these parameters are further increased following damage (109). Aside from histamine synthesis, HDC is able to regulate cholangiocyte proliferation by increasing VEGF expression and secretion via pERK signaling (109).

Histamine can signal through one of its four G protein-coupled receptors (H1-H4 HRs), and our lab has demonstrated that H1 and H2 HR activation increases, whereas H3 and H4 HR activation decreases, cholangiocyte proliferation (7, 16, 120). Specifically, H1HR acts via $G\alpha_q$, mobilizing Ca^{2+}, whereas H2HR signals through $G\alpha_s$, coupling to cAMP, and subsequent pERK activation (121, 122). Conversely, H3 and H4 HR activation decreases cAMP accumulation (123, 124). As previously stated, there is a prominent increase in large cholangiocyte H2HR expression in conjunction with increased biliary proliferation. In this same manuscript, we demonstrated that treatment with the H2HR antagonist, ranitidine, brought about a significant reduction in large duct mass along with decreased liver fibrosis (15). Since (i) PSC primarily affects the large ducts, (ii) H2HR is preferentially expressed on large cholangiocytes, (iii) activated MCs secrete large amounts of histamine, and (iv) infiltrating MCs reside in close proximity to large ducts, the aim of this study was to evaluate the impact of MC-derived histamine on large cholangiocyte damage via H2HR signaling.

CHAPTER II

METHODS*

Reagents and Materials

Reagents were purchased from Sigma Aldrich Co. (St. Louis, MO) unless otherwise indicated. Reagents for cell culture were obtained from Invitrogen Corporation (Carlsbad, CA). Total RNA was isolated from total liver, freshly isolated cells and cultured cells using the TRI Reagent from Sigma Life Science and was reverse transcribed with the Reaction Ready First Strand cDNA Synthesis kit (Qiagen, Valencia, CA).

Animal Models

We utilized commercially available homozygous mast cell-deficient C57BL/6J-*Kit*$^{W\text{-}sh}$/J (*Kit*$^{W\text{-}sh}$) mice obtained from Jackson Laboratory (Sacramento, CA) along with age-matched wild-type (WT) mice. Pair breeding was utilized to generate offspring and only male mice were used in our study. WT and *Kit*$^{W\text{-}sh}$ mice (at least 12 weeks of age) were subjected to sham or BDL (as described (8, 110)) for up to 7 days and, in separate experiments, *Kit*$^{W\text{-}sh}$ mice (at least 8 weeks of age) were injected with sterile, cultured MCs (MC/9 (ATCC® CRL-8306™)) or MC medium (control) prior to sacrifice 3 days later. At least 8-10 mice were used for each experimental group. Cultured MCs were tagged with PKH26 Red Fluorescent Cell Linker prior to injection and mice received a

*Part of this chapter is reprinted with permission from "Bile Duct Ligation-Induced Biliary Hyperplasia, Hepatic Injury, and Fibrosis Are Reduced in Mast Cell-Deficient *Kit*$^{W\text{-}sh}$ Mice" by Hargrove L, Kennedy L, Demieville J, Jones H, Meng F, DeMorrow S, Karstens W, Madeka T, Greene J Jr, Francis H, 2017. *Hepatology*, 65, 1991-2004, Copyright 2017 by John Wiley and Sons.

single injection of sterile, cultured MCs (5×10^6 cells in 0.1 ml sterile MC medium) or vehicle control via tail vein injection (125). Following euthanasia, the location of injected MCs was determined using confocal microscopy for the visualization of PKH26 Red Fluorescent Cell Linker. Livers were co-stained with CK-19 to mark bile ducts and aid in the location of injected MCs.

For a separate set of animal studies, we used the multidrug resistant genetically modified mouse model of PSC, *Mdr2*$^{-/-}$ mice raised on FVB/NJ background (wild-type, WT) (111). Male WT and *Mdr2*$^{-/-}$ mice were treated with either mismatch morpholino (TAAACCATGCAATTGGACTCAATTC) or an H2HR-specific Vivo Morpholino (TGAACCGTGCCATTGGGCTCCATTC) given by tail vein injection 2x/week for 1 week (4 μg/100 μl NaCl). Mice (8-10 per group) were euthanized at 8 and 12 weeks of age, times at which they display an increase in PSC-induced hepatic damage (15, 111).

All mice were housed in the Baylor Scott and White Health Animal Facility and given free access to drinking water and standard chow. Animals were kept in a temperature-controlled environment with a 12:12 hr light/dark cycle, and all protocols were approved by and strictly adhered to regulations set forth by the local IACUC committee. From all animals we collected serum, liver samples and isolated cholangiocytes. Cholangiocyte supernatants were collected and incubated at 37°C for up to 6 hours (37).

Analysis of Liver Damage

H&E staining was performed in liver sections to evaluate lobular damage, necrosis and inflammation. H&E staining was evaluated by a board-certified pathologist in a

blinded manner. Serum levels of alanine transaminase (ALT) and gamma-glutamyl transferase (γ-GT) were evaluated in certain groups of mice using the IDEXX Catalyst One test slides (IDEXX, Westbrook, ME).

Assessment of MC Presence and the Histamine/HR Axis

MC localization was assessed by immunohistochemistry for mouse mast cell protease-1 (mMCP-1) in liver sections, and gene expression of c-Kit, chymase and tryptase (MC markers) was measured in total liver by quantitative real-time PCR (*q*PCR). Histamine secretion was evaluated by EIA in serum from all groups using the Histamine EIA Kit (Cayman Chemical; Ann Arbor, MI). Expression levels of H1HR and H2HR were measured by immunohistochemistry or immunofluorescence (co-stained with CK-19 to label bile ducts) in liver sections.

Measurement of IBDM and Cholangiocyte Proliferation

Since increased intrahepatic bile duct mass (IBDM, indicative of ductular reaction) and cholangiocyte proliferation are found in BDL and *Mdr2*$^{-/-}$ mice, we evaluated these parameters in our models by immunohistochemistry with semi-quantification of CK-19 (13, 15). To further define whether MC presence modifies small or large bile duct mass, we again performed immunohistochemistry for CK-19 in liver sections and categorized bile duct mass into small (<14 μm diameter) or large ($\geq$14 μm diameter) ducts in our BDL studies and MC injection models. We have previously demonstrated that stimulation of H2HR enhances large, but not small, IBDM (15); therefore, we measured changes in

large IBDM in *Mdr2*$^{-/-}$ mice that were injected with H2HR Vivo Morpholino or mismatch controls.

Evaluation of Kupffer Cell Number, HSC Activation, Hepatic Fibrosis and Angiogenesis

Increased Kupffer cell presence has been noted in various models of cholestasis, as well as in humans with cholestatic injury (23, 126). To evaluate changes in Kupffer cell number, liver sections were stained for F4/80 (Kupffer cell marker).

HSCs are the key contributors to hepatic fibrosis during liver injury, and increased HSC number has been seen in a number of cholestatic injury models (11, 27, 32, 36). To evaluate if MC presence correlates with increased HSC number and activation, we performed immunofluorescence in liver sections for desmin (HSC marker) co-stained for CK-19 (to image bile ducts). To investigate if blocking H2HR signaling alters HSC activation, we again visualized the expression of synaptophysin-9 (SYP-9, marker of activated HSCs) by immunofluorescence, co-stained for CK-19. To determine changes in liver fibrosis, that are mediated by HSCs, we performed staining in liver sections using Masson's Trichrome and Sirius Red (semi-quantified), and *q*PCR for α-SMA, fibronectin-1 (FN-1) and collagen type-1a in total liver RNA.

TGF-β1 is a strong regulator of HSC activation and hepatic fibrosis. We measured TGF-β1 signaling in our models by (i) hepatic and isolated large cholangiocyte expression by *q*PCR, (ii) hepatic expression by immunofluorescence (co-stained for CK-19 to image bile ducts) and (iii) secretion in serum by EIA.

Vascular remodeling was visualized in our models by immunofluorescence for von Willebrand factor (vWF) and CK-19 (to image bile ducts). As well, the gene expression of vWF was determined in total liver RNA by *q*PCR. VEGF-C expression in isolated large cholangiocytes was verified by *q*PCR. Expression and secretion of VEGF-A in large cholangiocyte supernatants was determined by *q*PCR and EIA, respectively.

Visualization of Intracellular Signaling

Our previous work has shown that H2HR signals primarily through activation of $G\alpha_s$/cAMP/pERK; therefore, we evaluated this signaling pathway in our mouse models. Intracellular cAMP and pERK expression were determined by immunofluorescence (co-stained with CK-19 to visualize localization within bile ducts). These results were evaluated for changes in small versus large bile ducts based on bile duct diameter as described above.

***In Vitro* Methods**

Since we have found that MCs primarily reside near large ducts, we wanted to investigate whether damaged cholangiocytes (small versus large) induced the migration of MCs *in vitro*. For these studies, we utilized our immortalized, large mouse cholangiocyte cell lines and immortalized, small mouse cholangiocyte cell lines that were generated by SV-40 transformation and previously used by us (3), as well as a fetal mouse liver MC line (MC/9, ATCC) also previously used by us (15, 36). Immortalized small and large cholangiocytes were treated with of lipopolysaccharide (LPS, 100 ng/mL) for 24 hrs (to induce damage) prior to being placed in the bottom well of Boyden

chambers; the top well was loaded with cultured MCs and migration through transwell membranes was assessed 24 hrs later by counting toluidine blue-positive cells (94).

We have previously demonstrated that H2HR expression is primarily in large cholangiocytes (15); therefore, we wanted to evaluate the impact of MC-derived histamine on large cholangiocyte proliferation and damage. We performed all *in vitro* studies using our immortalized, large mouse cholangiocyte cell lines and our cultured MC cell line. *In vitro*, MCs were treated with either 0.1% BSA (control) or an HDC inhibitor (3 mM, α-methyl-DL-histidine (α-Me)) for 48 hrs. Large cholangiocytes were treated with supernatants from treated MCs and were evaluated for (i) proliferation by Ki67 staining, (ii) senescence by p18 immunofluorescent staining, and (iii) H2HR/pERK signaling by immunofluorescent staining.

Lastly, we wanted to demonstrate that large cholangiocytes treated with MC supernatants were acting through cAMP signaling. *In vitro*, large cholangiocytes were treated with supernatants from control- or α-Me-treated MCs, and were assessed for intracellular cAMP levels using the Cyclic AMP ELISA Kit (Cayman Chemical, Ann Arbor, MI).

Statistical Methods

All data is expressed as mean ± standard error of the mean (SEM). Groups were analyzed by the Student unpaired t test when two groups are analyzed or a two-way ANOVA when more than two groups are analyzed, followed by an appropriate post hoc test. A p value <0.05 was considered statistically significant.

CHAPTER III

RESULTS*

Injected MCs are Found in Close Proximity to Bile Ducts

We first verified that our injection model was able to efficiently deliver MCs to the liver. We found few injected MCs in the lung and spleen; however, injected MCs were found in the liver and in close proximity to bile ducts (Figure 1).

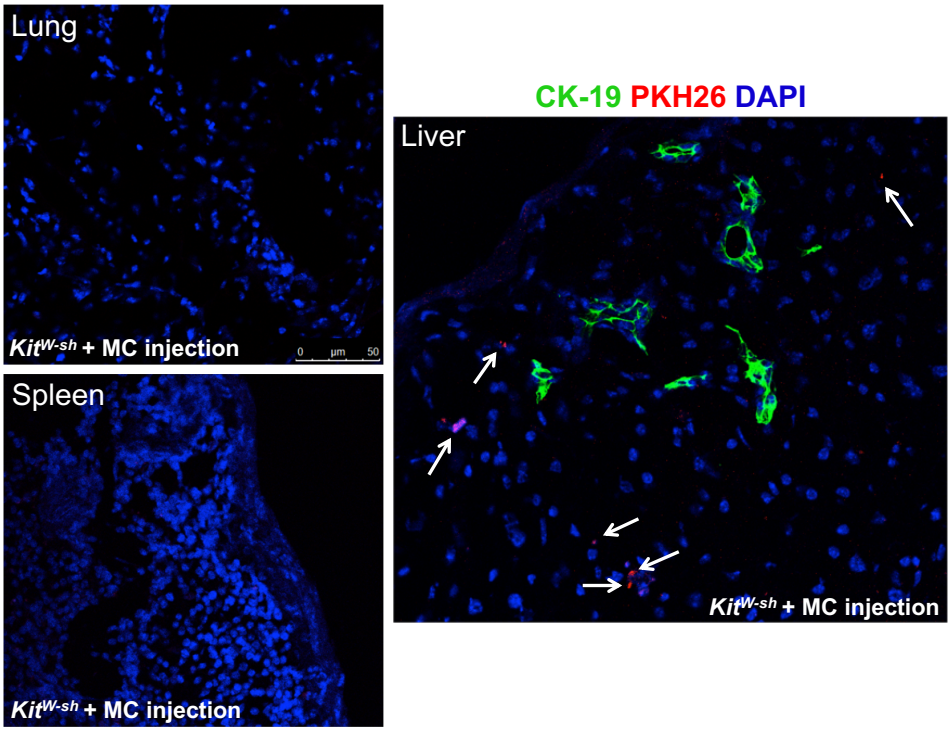

Figure 1, MC Localization Following Tail Vein Injection. MC localization following tail vein injection was determined in *Kit*$^{W\text{-}sh}$ mice. Confocal imaging for PKH26 (red) in the lungs, spleens and livers from *Kit*$^{W\text{-}sh}$ mice injected with sterile PKH26-tagged MCs reveals that the majority of injected MCs (white arrows) are in the liver and not found in lung or spleen. Livers were co-stained with CK-19 (green) to mark bile ducts for MC localization. Images are 20× magnification.

---

*Part of this chapter is reprinted with permission from "Bile Duct Ligation-Induced Biliary Hyperplasia, Hepatic Injury, and Fibrosis Are Reduced in Mast Cell-Deficient *Kit*$^{W\text{-}sh}$ Mice" by Hargrove L, Kennedy L, Demieville J, Jones H, Meng F, DeMorrow S, Karstens W, Madeka T, Greene J Jr, Francis H, 2017. *Hepatology*, 65, 1991-2004, Copyright 2017 by John Wiley and Sons.

Hepatic Injury is Ameliorated in BDL *Kit$^{W\text{-}sh}$* Mice

BDL WT mice displayed increased focal necrosis (infarct) in zone 2 (upwards of 4–5% of lobule) and portal inflammatory changes that are consistent with obstruction (Figure 2A, indicated by black arrowheads). An increase in mostly large bile ducts is also observed following BDL (indicated by black arrows) in WT mice. In BDL *Kit$^{W\text{-}sh}$* mice the degree of focal necrosis (infarct) was zero compared to BDL WT mice. ALT activity was significantly upregulated in BDL WT mice, but this increase was completely abolished in the BDL *Kit$^{W\text{-}sh}$* mice, which demonstrated ALT levels similar to those in sham WT mice (Figure 2B). These findings support previously reported findings that BDL primarily induces large duct damage, which is ameliorated when MCs are absent.

MC Injection Does Not Recapitulate BDL-Induced Hepatic Injury in *Kit$^{W\text{-}sh}$* Mice

To evaluate whether MC injections recapitulate BDL-induced damage, we re-injected MCs into MC-deficient (*Kit$^{W\text{-}sh}$*) mice and evaluated the same parameters. In the livers of *Kit$^{W\text{-}sh}$* mice injected with MCs there were no visible areas of liver infarcts/focal necrosis or portal inflammation/damage compared to *Kit$^{W\text{-}sh}$* mice injected with PBS (Figure 2C). Further, ALT levels were not significantly altered after MC injection compared to controls, suggesting that introduction of MCs does not mimic BDL-induced damage (Figure 2D).

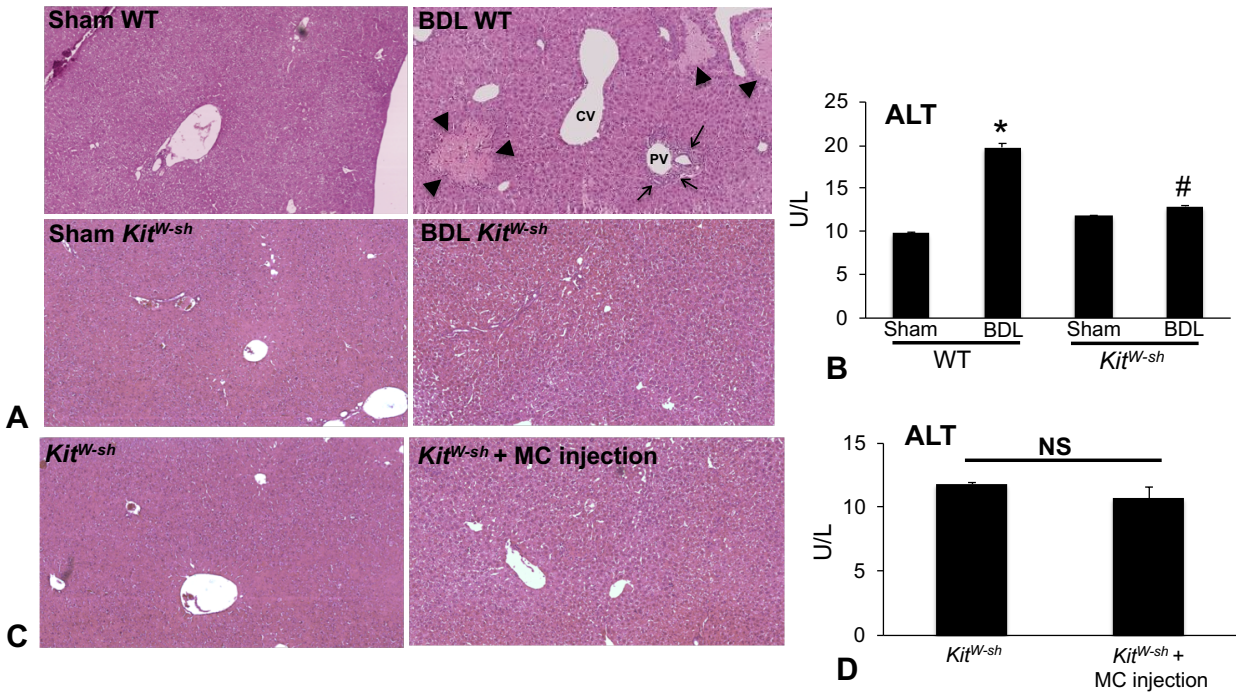

Figure 2, Analysis of Liver Damage. Liver damage was assessed by H&E staining of liver sections from all groups. BDL WT mice had increased focal necrosis (infarct) indicated by black arrowheads (upwards of 4–5% of lobule) and portal inflammatory changes that are consistent with obstruction. An increase in mostly large bile ducts is observed following BDL (indicated by black arrows). In *Kit*$^{W\text{-}sh}$ sham mice and *Kit*$^{W\text{-}sh}$ mice subjected to BDL, necrosis/liver infarcts were absent (A). ALT activity was increased in BDL WT compared to sham WT, whereas ALT activity in both sham and BDL *Kit*$^{W\text{-}sh}$ sham mice was similar to sham WT (B). *Kit*$^{W\text{-}sh}$ mice injected with MCs had no visible areas of liver necrosis/infarcts or portal inflammation/damage compared to *Kit*$^{W\text{-}sh}$ mice injected with control (C) and ALT levels were unchanged (D). Data are expressed as mean ± SEM of at least 6 experiments for ALT. *p<0.05 versus sham WT mice; #p<0.05 versus BDL WT mice. Images are 10× magnification. PV = portal vein; CV = central vein.

IBDM and Cholangiocyte Proliferation are Significantly Reduced in BDL *Kit*$^{W\text{-}sh}$ Mice

In line with our previous publications, BDL WT mice had an increase in IBDM compared to sham WT mice. However, in BDL *Kit*$^{W\text{-}sh}$ mice there is an overall reduction in IBDM compared to BDL WT mice (Figure 3A). These results were further confirmed by western blotting (Figure 3B) and *q*PCR (Figure 3C) using total liver samples,

demonstrating a similar trend to that noted in the immunohistochemistry results. As expected, biliary proliferation (indicated by red arrows), evaluated by Ki-67 staining, was significantly decreased in BDL *Kit*$^{W\text{-}sh}$ mice compared to BDL WT (Figure 4). However, cholangiocyte proliferation was similar between sham WT and *Kit*$^{W\text{-}sh}$ mice (Figure 4). These data demonstrate that MCs mediate cholangiocyte proliferation during BDL.

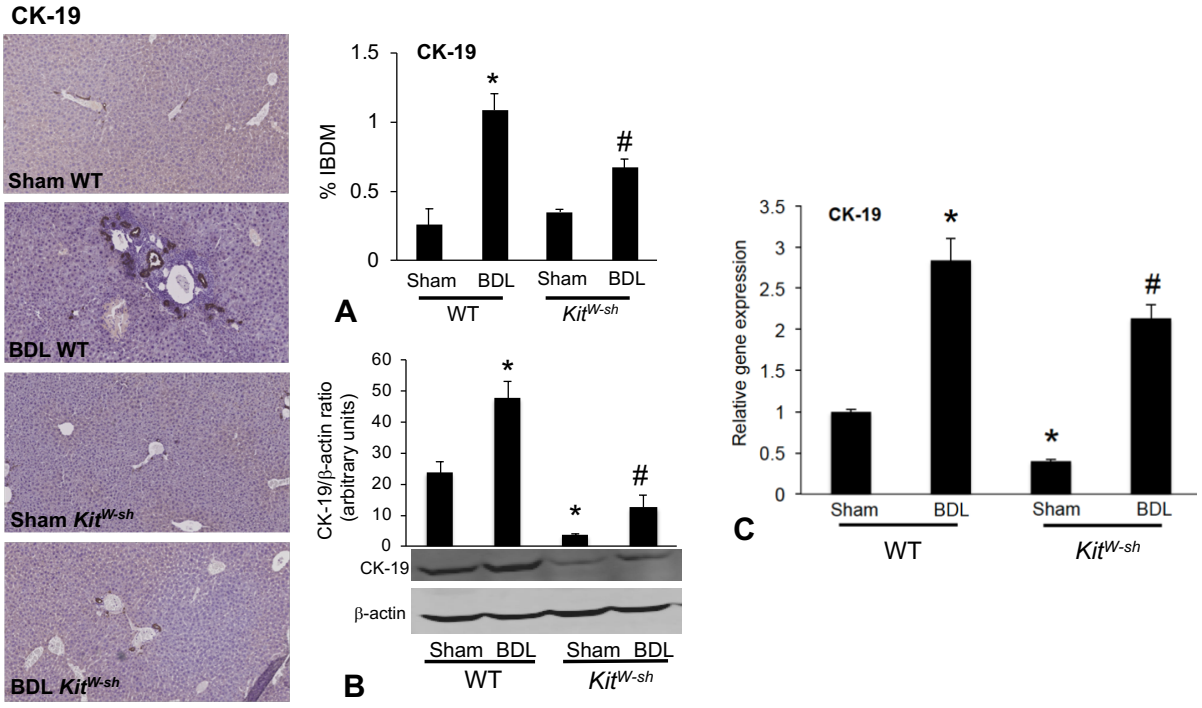

Figure 3, Evaluation of IBDM Following BDL. IBDM (A and B) was evaluated in liver sections from WT and *Kit*$^{W\text{-}sh}$ subjected to sham and BDL surgery. We found that IBDM (assessed by CK-19 staining (A), western blotting (B) and *q*PCR (C)) increased in BDL WT mice when compared to sham WT mice, whereas IBDM was reduced in BDL *Kit*$^{W\text{-}sh}$ mice. Semi-quantitative data is expressed as mean ± SEM of at least 10 experiments for CK-19, at least 8 experiments for western blotting and 4 experiments for *q*PCR. *p<0.05 versus sham WT mice; #p<0.05 versus BDL WT mice. Images are 10× magnification.

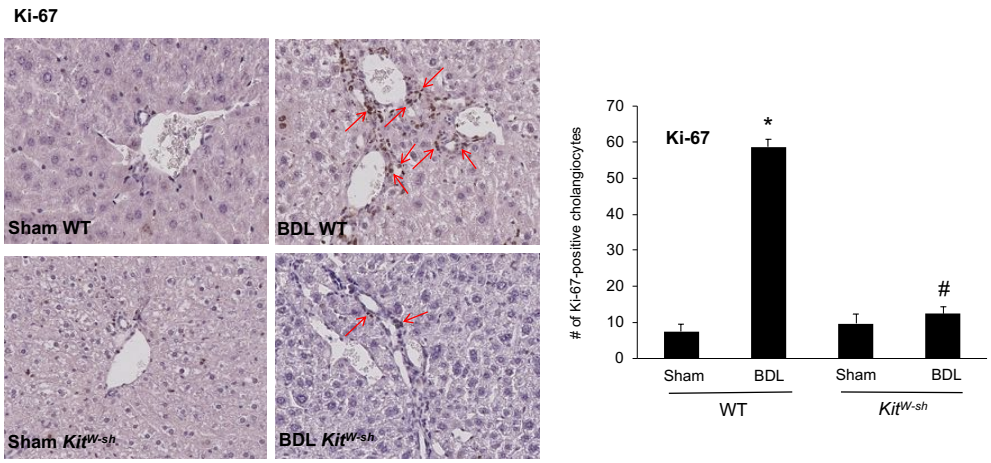

Figure 4, Assessment of Cholangiocyte Proliferation Following BDL. Cholangiocyte proliferation was evaluated in liver sections from WT and *Kit*$^{W\text{-}sh}$ subjected to sham and BDL surgery. We found that cholangiocyte proliferation (red arrows), as indicated by Ki-67 staining, increased in BDL WT mice when compared to sham WT mice, whereas the number of proliferating cholangiocytes was reduced in BDL *Kit*$^{W\text{-}sh}$ mice. Semi-quantitative data are expressed as mean ± SEM of at least 10 experiments. *p<0.05 versus sham WT mice; #p<0.05 versus BDL WT mice. Images are 20× magnification.

MC Injection Increases IBDM and Cholangiocyte Proliferation in *Kit*$^{W\text{-}sh}$ Mice

When looking at our MC injection models, we found that *Kit*$^{W\text{-}sh}$ mice injected with MCs had a significant increase in IBDM when compared to *Kit*$^{W\text{-}sh}$ mice (Figure 5A). Similarly, cholangiocyte proliferation was increased in *Kit*$^{W\text{-}sh}$ mice injected with MCs when compared to controls (Figure 5B). CK-19 expression was further confirmed by *q*PCR (Figure 5C) and western blotting (Figure 5D) using total liver samples.

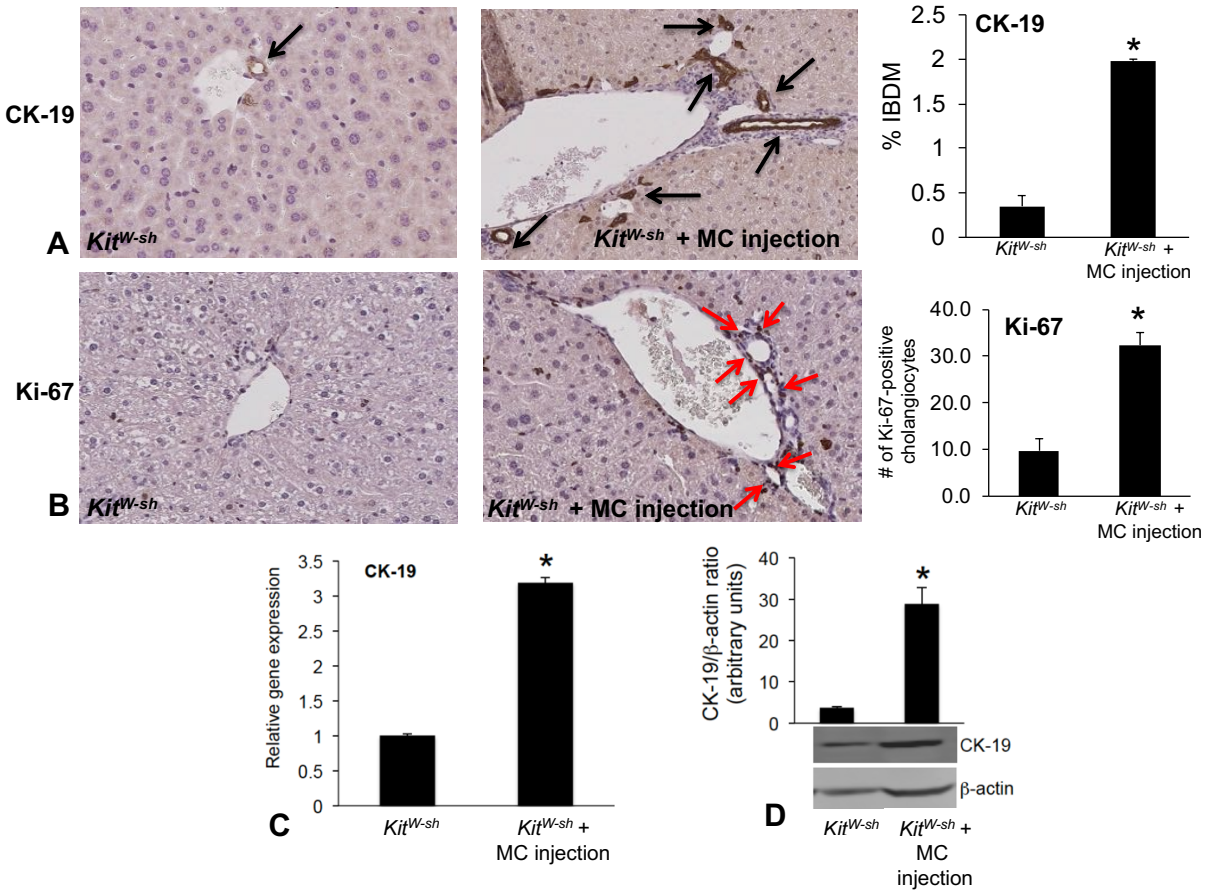

Figure 5, Evaluation of IBDM and Cholangiocyte Proliferation Following MC Injection. Evaluation of IBDM and proliferation following the MC injection into *Kit*$^{W\text{-}sh}$ mice. (A) IBDM and (B) biliary proliferation are increased in *Kit*$^{W\text{-}sh}$ mice injected with MCs compared to control injections as shown by CK-19 (marked by black arrows) and Ki67 (marked by red arrows). *Kit*$^{W\text{-}sh}$ mice injected with MCs have an increase in CK-19 gene expression compared to mice injected with vehicle (C) that was confirmed by western blotting (D). Data are expressed as mean ± SEM of 10 experiments for CK-19, 4 experiments for *q*PCR and 8 experiments for western blotting. *p<0.05 versus *Kit*$^{W\text{-}sh}$ mice. Images are 20× magnification.

MCs Influence Large, But Not Small, IBDM During BDL and Following MC Injection into *Kit*$^{W\text{-}sh}$ Mice

As previously stated, BDL induces the proliferation of large, but not small, cholangiocytes, thereby increasing large duct mass. When evaluating the differential impact of MCs on small versus large duct mass, we found that BDL *Kit*$^{W\text{-}sh}$ mice had a

significant reduction in large IBDM when compared to BDL WT mice; however, there was a slight but significant increase in small IBDM in BDL *Kit*$^{W\text{-}sh}$ mice as compared to sham *Kit*$^{W\text{-}sh}$ mice (Figure 6). Interestingly, we noted that sham *Kit*$^{W\text{-}sh}$ mice had a reduction in large IBDM, but an increase in small IBDM, when compared to sham WT mice (Figure 6). These findings suggest that MC presence mediates large cholangiocyte proliferation, and loss of MCs leads to a reduction in large cholangiocyte growth with an increase in small cholangiocyte proliferation to compensate for the loss in biliary growth.

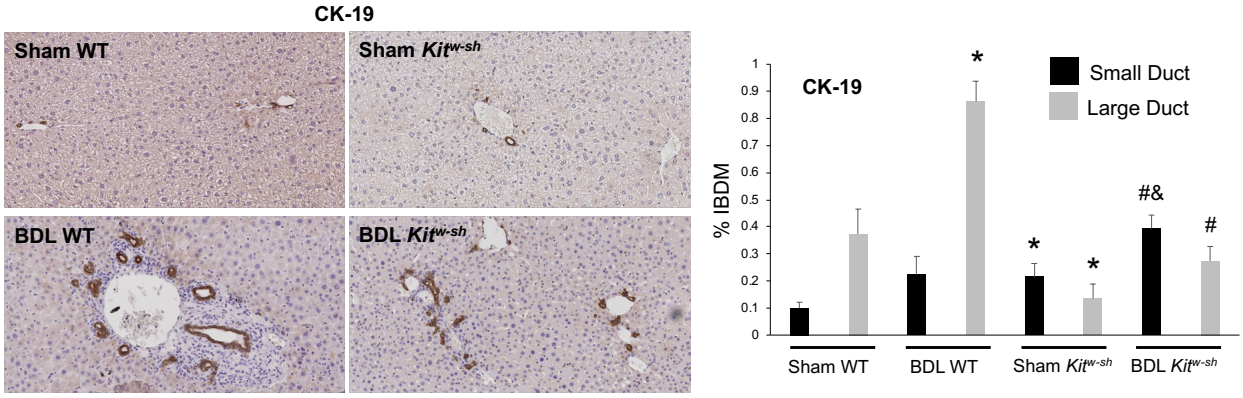

Figure 6, Determination of Small and Large IBDM Following BDL. Small and large IBDM was determined in liver sections from WT and *Kit*$^{W\text{-}sh}$ mice subjected to sham and BDL surgery. By CK-19 staining, we noted that large (but not small) IBDM was increased in BDL WT mice when compared to sham WT mice; however, large IBDM was reduced in BDL *Kit*$^{W\text{-}sh}$ mice when compared to BDL WT mice, with a compensatory increase in small duct mass when compared to sham *Kit*$^{W\text{-}sh}$ mice. Interestingly, sham *Kit*$^{W\text{-}sh}$ mice had a significant increase in small duct mass, with a significant decrease in large duct mass, when compared to sham WT mice. Semi-quantitative data is expressed as mean ± SEM of at least 10 experiments for CK-19. *p<0.05 versus sham WT mice; #p<0.05 versus BDL WT mice; &p<0.05 versus sham *Kit*$^{W\text{-}sh}$ mice. Images are 10× magnification.

Interestingly, we found that the injection of MCs into WT mice did not significantly alter small or large IBDM (Figure 7). The injection of MCs into *Kit*$^{W\text{-}sh}$ mice was able to

increase large IBDM with a slight increase in small IBDM; however, the change in small duct mass was not as prominent as the change in large duct mass (Figure 7). Therefore, we propose that MCs primarily target large cholangiocyte proliferation during models of cholestasis. Additionally, since MC injection modified large duct mass in *Kit*$^{W\text{-}sh}$ mice, but not WT, we utilized the *Kit*$^{W\text{-}sh}$ mice for our MC injection studies.

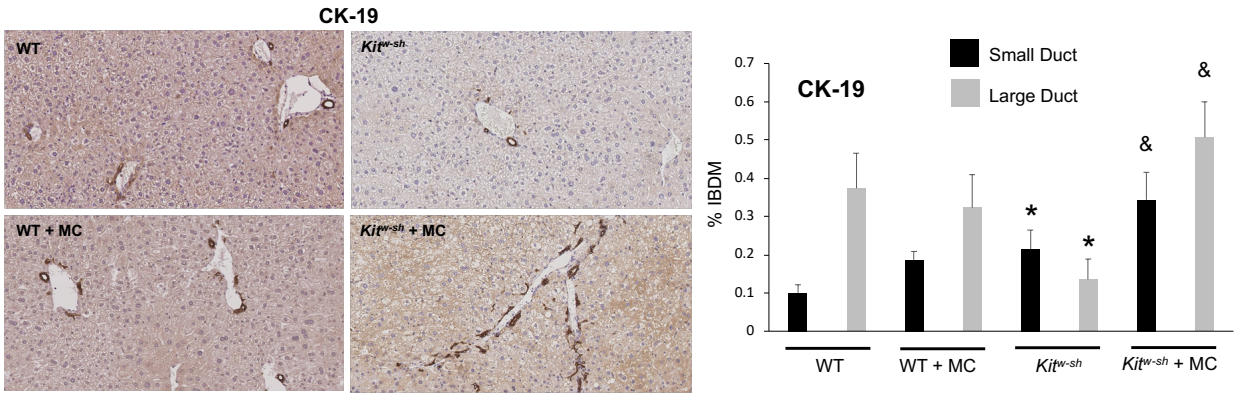

Figure 7, Measurement of Small and Large Cholangiocyte Proliferation Following MC Injection. Small and large IBDM was evaluated in liver sections from MC injection mice. By CK-19 staining, we found that WT mice injected with MCs had no significant change in small or large IBDM when compared to WT mice injected with control. Similarly, the injection of MCs into *Kit*$^{W\text{-}sh}$ mice increased both small and large IBDM, with a more prominent increase in large duct mass, when compared to *Kit*$^{W\text{-}sh}$ mice injected with control. Semi-quantitative data is expressed as mean ± SEM of 10 experiments for CK-19. *p<0.05 versus WT mice; &p<0.05 versus *Kit*$^{W\text{-}sh}$ mice. Images are 20× magnification.

MCs Increase Kupffer Cell Number During BDL and Following MC Injection into *Kit*$^{W\text{-}sh}$ Mice

Kupffer cell number is increased in BDL and *Mdr2*$^{-/-}$ mice (23, 126). Using F4/80 staining, we found that BDL *Kit*$^{W\text{-}sh}$ mice had a significant reduction in Kupffer cell number when compared to BDL WT mice (Figure 8). Kupffer cell number was unchanged between

WT and *Kit*$^{W\text{-}sh}$ mice subjected to sham operation (Figure 8). However, MC injection into *Kit*$^{W\text{-}sh}$ mice increased Kupffer cell presence when compared to control mice (Figure 8).

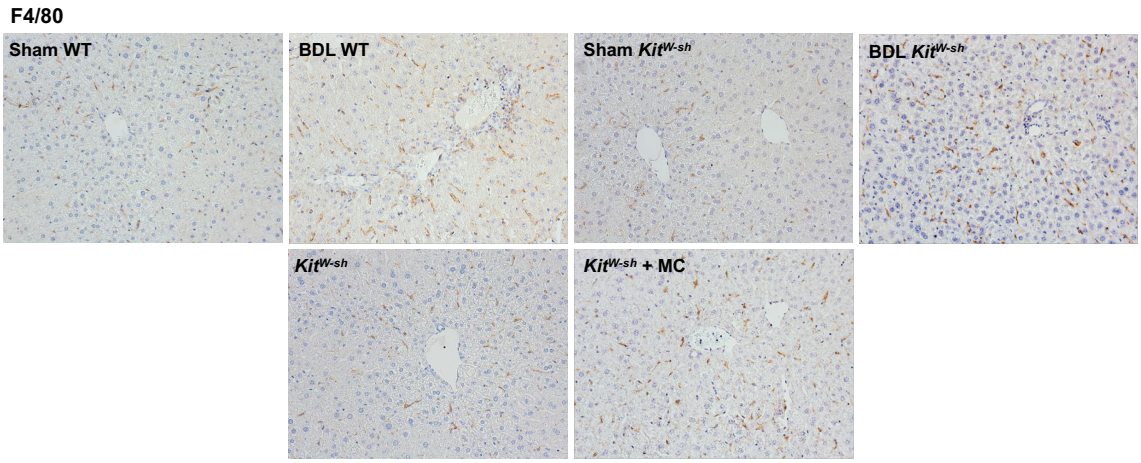

Figure 8, Visualization of Kupffer Cell Number Following BDL or MC Injection. Kupffer cell number was assessed by staining for F4/80 (Kupffer cell marker) in liver sections. We found that BDL WT mice had an increase in Kupffer cell number when compared to sham WT mice; however, BDL *Kit*$^{W\text{-}sh}$ mice had a decrease in Kupffer cell number when compared to BDL WT mice. The injection of MCs into *Kit*$^{W\text{-}sh}$ mice increased Kupffer cell number when compared to control injected *Kit*$^{W\text{-}sh}$ mice. Images are 20× magnification.

Hepatic Fibrosis and HSC Activation Are Dependent on MCs

Collagen deposition is dramatically reduced in BDL *Kit*$^{W\text{-}sh}$ mice compared to BDL WT mice as shown by Masson's Trichrome and Sirius Red staining (Figure 9A and B). Semi-quantification of Sirius Red staining shows a significant decrease in collagen deposition in BDL *Kit*$^{W\text{-}sh}$ mice compared to BDL WT mice (Figure 9C). Hydroxyproline content was significantly reduced in BDL *Kit*$^{W\text{-}sh}$ mice compared to BDL WT mice (Figure 9D). The expression of α-SMA, fibronectin-1 and collagen type-1a increased in BDL WT

mice compared to sham WT mice; whereas, these markers were decreased in BDL *Kit*$^{W\text{-}sh}$ mice compared to BDL WT mice (Figure 10).

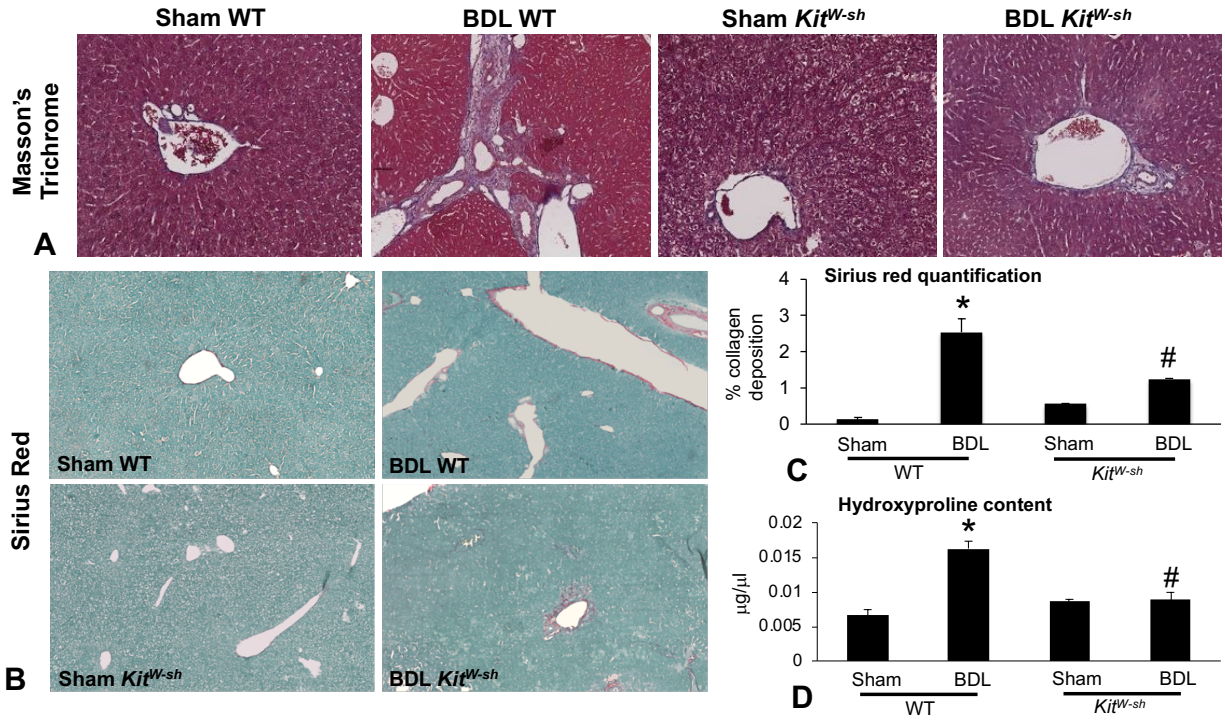

Figure 9, Evaluation of Hepatic Fibrosis Following BDL. Fibrosis was evaluated by staining in WT and *Kit*$^{W\text{-}sh}$ mice subjected to sham or BDL surgery. (A) Masson's Trichrome and (B) Sirius Red staining show an increase in collagen deposition in BDL WT mice compared to sham WT mice, whereas collagen deposition is reduced in BDL *Kit*$^{W\text{-}sh}$ mice compared to BDL WT mice. (C) The Sirius Red findings were quantified and presented as percent collagen deposition. (D) Hydroxyproline content in total liver was significantly increased in BDL WT mice compared to sham WT mice, but this was reduced in BDL *Kit*$^{W\text{-}sh}$ mice compared to BDL WT mice. Data are expressed as mean ± SEM of 6 experiments for hydroxyproline content and 10 images for Sirius Red. *p<0.05 versus sham WT mice; #p<0.05 versus BDL WT mice. Images are 10× magnification for Sirius Red and 20× for Masson's Trichrome.

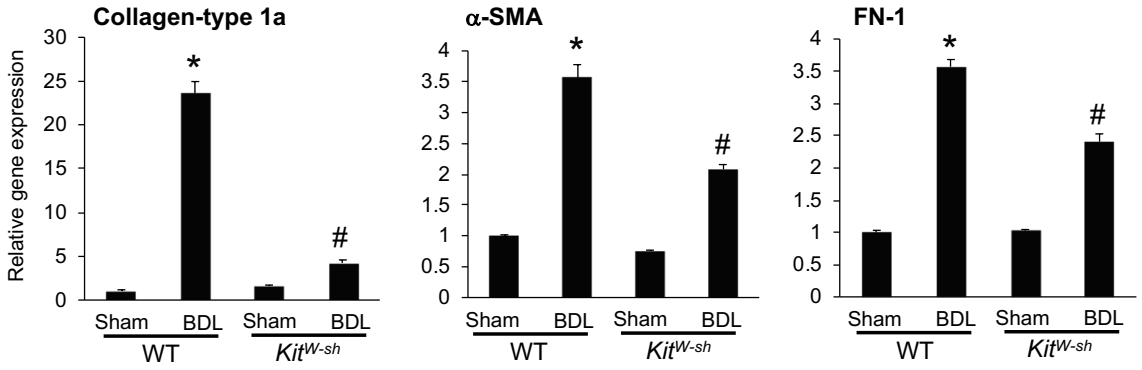

Figure 10, Expression of Fibrosis Genes Following BDL. Evaluation of fibrotic marker gene expression in WT and *Kit*$^{W\text{-}sh}$ mice subjected to sham or BDL surgery. Expression of collagen type-1a, α-SMA, and fibronectin-1 (FN-1) genes were measured by *q*PCR and all three were upregulated in BDL WT mice compared to sham WT mice. These fibrosis markers were decreased in BDL *Kit*$^{W\text{-}sh}$ mice compared to BDL WT mice. Data are expressed as mean ± SEM of at least 9 experiments for real-time PCR. *p<0.05 versus sham WT mice; #p<0.05 versus BDL WT mice.

TGF-β1 is a key promoter of liver fibrosis via HSC activation; therefore, we measured both of these parameters in our models. In BDL *Kit*$^{W\text{-}sh}$ mice, there was a significant reduction in both TGF-β1 expression (Figure 11A) and secretion (Figure 11B) compared to BDL WT mice. Similarly, the number of HSCs, as demonstrated by desmin (HSC marker) expression, was increased in BDL WT mice, but reduced in BDL *Kit*$^{W\text{-}sh}$ mice (Figure 12).

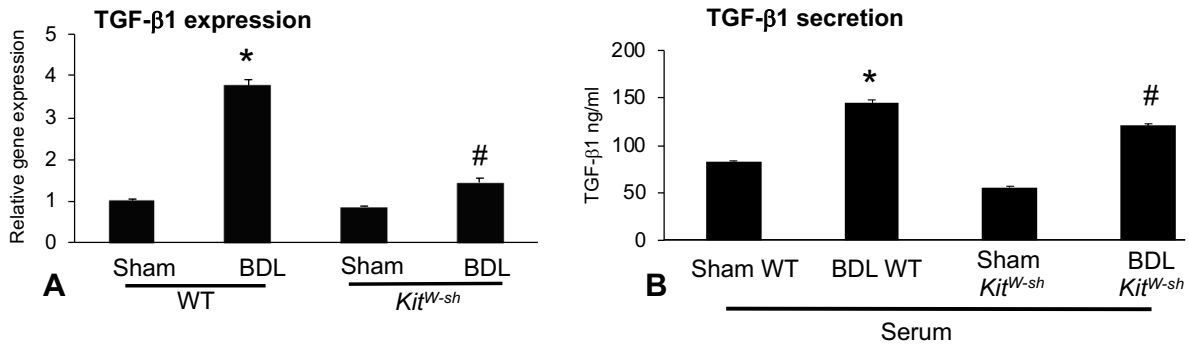

Figure 11, Assessment of TGF-β1 Levels Following BDL. Measurement of TGF-β1 expression in WT and *Kit*$^{W\text{-}sh}$ mice subjected to sham or BDL surgery. (A) TGF-β1 gene expression and (B) secretion are increased in BDL WT mice compared to sham WT mice, whereas both expression and secretion of TGF-β1 are decreased in BDL *Kit*$^{W\text{-}sh}$ mice compared to BDL WT mice. (C) Data are expressed as mean ± SEM of 6 experiments for *q*PCR and at least 3 experiments run in triplicates for EIA. *p<0.05 versus sham WT mice; #p<0.05 versus BDL WT mice.

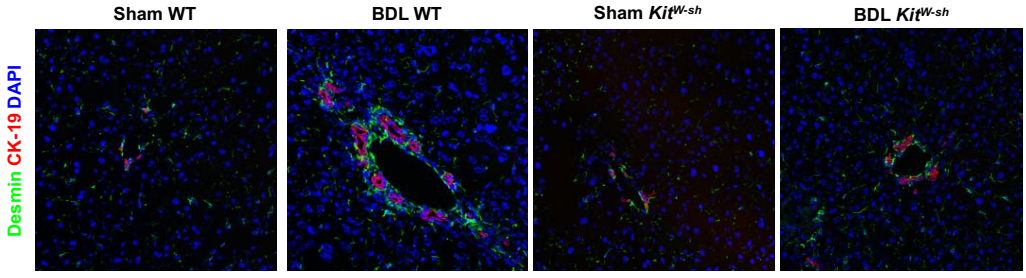

Figure 12, Visualization of HSC Activation Following BDL. Visualization of HSC activation assessed using desmin expression in WT and *Kit*$^{W\text{-}sh}$ mice subjected to sham or BDL surgery. The number of desmin-positive HSCs (stained green) was increased in BDL WT mice when compared to sham WT mice, but this was reduced in BDL *Kit*$^{W\text{-}sh}$ mice when compared to BDL WT mice. Images are 40× magnification.

It has been demonstrated that blocking MC activation reduces hepatic fibrosis and HSC activation in *Mdr2*$^{-/-}$ mice (15, 37, 100). We next evaluated if injection of MCs is able to increase these parameters, and we found that reintroduction of MCs into *Kit*$^{W\text{-}sh}$ mice

increased collagen deposition (Figure 13) and HSC activation (Figure 14) when compared to vehicle-injected mice.

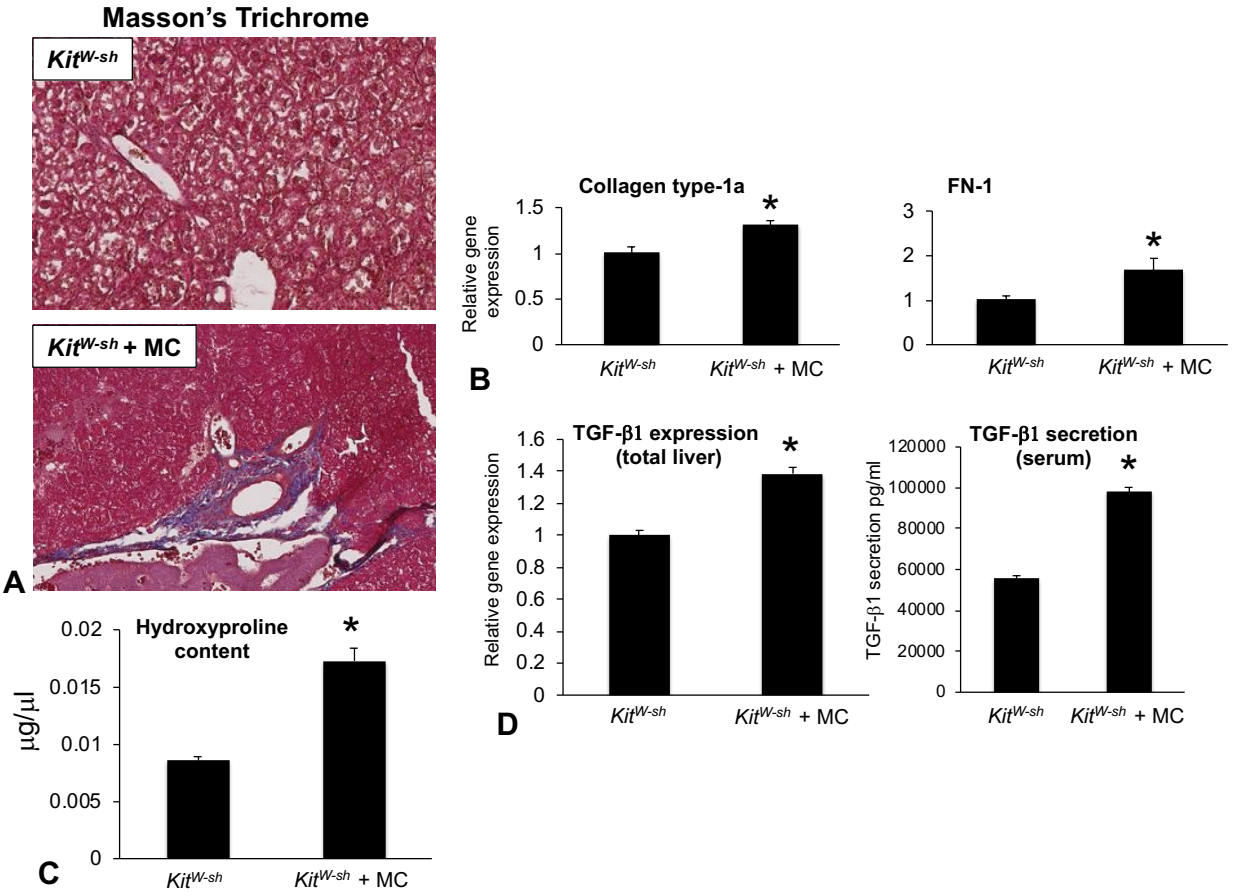

Figure 13, Determination of Liver Fibrosis and TGF-β1 Levels Following MC Injection. Measurement of liver fibrosis following the reintroduction of MCs into MC-deficient, *Kit*$^{W\text{-}sh}$ mice. (A) Masson's Trichrome staining reveals an increase in collagen deposition in *Kit*$^{W\text{-}sh}$ mice injected with MCs compared to 1X PBS. (B) Gene expression of fibrotic markers (collagen type-1a and fibronectin-1) are increased in *Kit*$^{W\text{-}sh}$ mice injected with MCs compared to control injections and (C) hydroxyproline content is increased following injection with MCs compared to control. (D) TGF-β1 expression and secretion are upregulated in *Kit*$^{W\text{-}sh}$ mice injected with MCs compared to control injections. Data are expressed as mean ± SEM of at least 6 experiments for *q*PCR and at least 3 experiments run in triplicate for EIA. *p<0.05 versus *Kit*$^{W\text{-}sh}$ mice injected with 1X PBS. Images are 20× magnification.

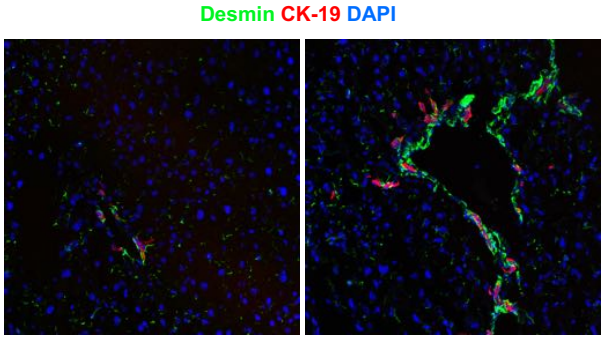

Figure 14, Visualization of HSC Activation Following MC Injection. Visualization of HSC activation by desmin expression in following MC injection into *Kit*$^{W\text{-}sh}$ mice. The number desmin-positive HSCs was increased in *Kit*$^{W\text{-}sh}$ mice injected with MCs when compared to control injected mice. Images are 40× magnification.

Histamine Signaling and Secretion Are Decreased in BDL *Kit*$^{W\text{-}sh}$ Mice

In BDL WT mice, there was increased serum histamine levels alongside increased hepatic H1 and H2 HR gene expression when compared to sham WT mice; however, in BDL *Kit*$^{W\text{-}sh}$ mice these parameters were decreased (Figure 15 A-C).

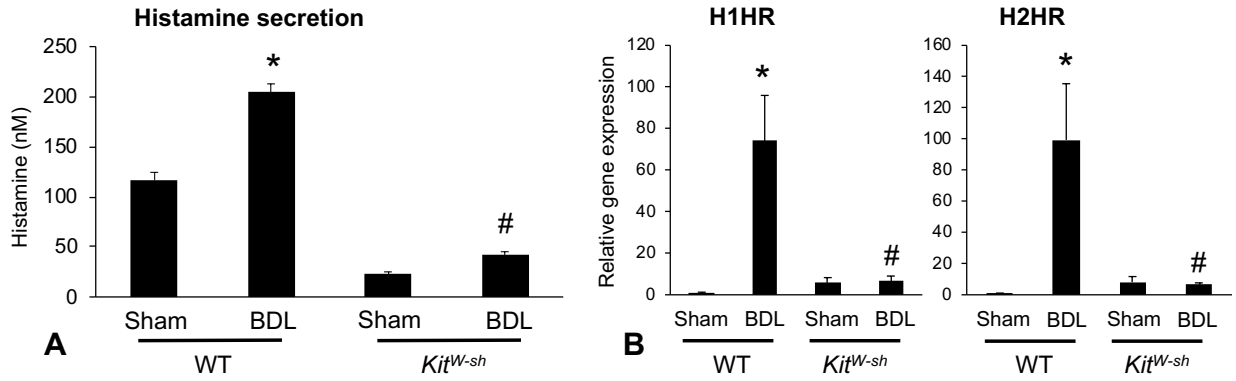

Figure 15, Measurement of Histamine Secretion and H1/H2 HR Expression Following BDL. Measurement of histamine secretion and H1/H2 HR expression in WT and *Kit*$^{W\text{-}sh}$ mice subjected to sham or BDL surgery. (A) Histamine secretion is upregulated in serum from BDL WT mice compared to sham WT mice, whereas histamine secretion from BDL *Kit*$^{W\text{-}sh}$ mice serum is significantly decreased compared to BDL WT mouse serum. (B) H1 and H2 HR gene expression is increased in BDL WT mice compared to sham WT mice, whereas gene expression of H1 and H2 HR are decreased in BDL *Kit*$^{W\text{-}sh}$ mice compared to BDL WT. Data are expressed as mean ± SEM of 3 experiments run in triplicate for EIA and 6 experiments for *q*PCR. *p<0.05 versus sham WT mice; #p<0.05 versus BDL WT mice.

We next wanted to specifically evaluate changes in H1HR and H2HR expression in small and large cholangiocytes in our models. First, we found a minimal increase in H1HR expression in small cholangiocytes, with no change in large cholangiocytes following BDL (Figure 16A). Interestingly, there was an upregulation in H1HR expression in peripheral, non-biliary cells (Figure 16A). However, we saw a strong and significant increase in H2HR predominantly in large cholangiocytes in BDL WT mice when compared to sham WT mice (Figure 16B). The expression of both H1HR and H2HR in these various cell types was significantly reduced in BDL *Kit*$^{W\text{-}sh}$ mice when compared to BDL WT mice (Figure 16A and B). Since we primarily found an upregulation in H2HR in large cholangiocytes, we evaluated the downstream effectors, cAMP and pERK in these cells. We saw a similar trend wherein large cholangiocyte cAMP/pERK expression was increased in BDL WT mice when compared to sham WT mice, but was significantly

reduced in large cholangiocytes in BDL *Kit*$^{W\text{-}sh}$ mice when compared to BDL WT mice (Figure 16C and D).

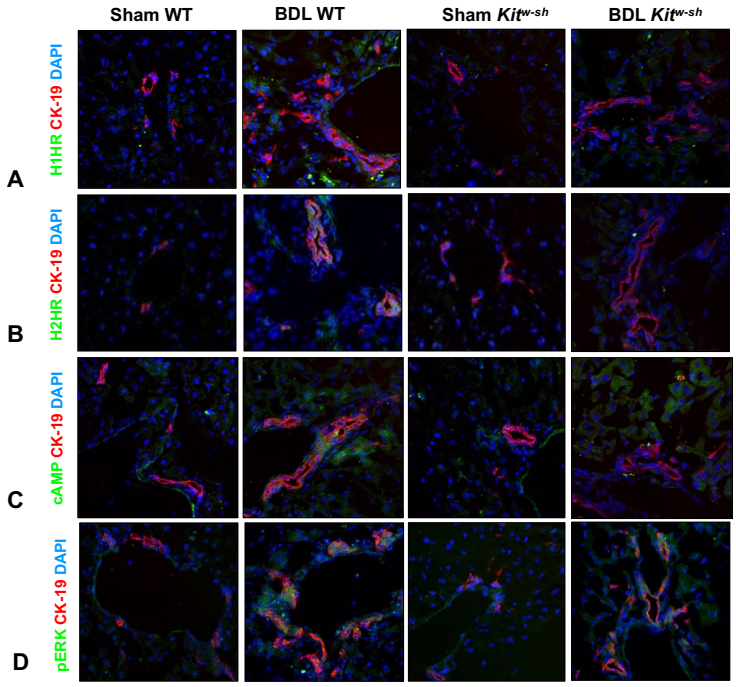

Figure 16, Assessment of cAMP/pERK Expression Following BDL. Evaluation of H1HR, H2HR and cAMP/pERK expression in WT and *Kit*$^{W\text{-}sh}$ mice subjected to sham or BDL surgery. (A) H1HR expression is increased in small ducts and peripheral, non-biliary cells in BDL WT mice when compared to sham WT mice; however, H1HR expression is decreased in BDL *Kit*$^{W\text{-}sh}$ mice when compared to BDL WT mice. (B) H2HR expression is strongly and predominantly increased in large ducts in BDL WT mice when compared to sham WT mice, but this is reduced in BDL *Kit*$^{W\text{-}sh}$ mice. (C) Large duct expression of cAMP is upregulated in BDL WT mice when compared to sham WT mice, but decreased in large ducts of BDL *Kit*$^{W\text{-}sh}$ mice. (D) Similarly, pERK expression in large ducts is increased in BDL WT mice when compared to sham WT mice; however, this is significantly decreased in BDL *Kit*$^{W\text{-}sh}$ mice. Images are 80× magnification.

MC Injection Increases HR Signaling in *Kit*$^{W\text{-}sh}$ Mice

We next evaluated whether the injection of MCs is able to restore H1/H2 HR and cAMP/pERK expression in MC-deficient mice. As expected, the injection of MCs minimally increased H1HR expression in small cholangiocytes and peripheral cells in *Kit*$^{W\text{-}}$

^{sh} mice (Figure 17A). Interestingly, MC injection increases hepatic H2HR expression in *Kit*$^{W\text{-}sh}$ mice (Figure 17B). As well, *Kit*$^{W\text{-}sh}$ mice have increased cAMP and pERK expression found primarily in large versus small cholangiocytes (Figure 17C and D).

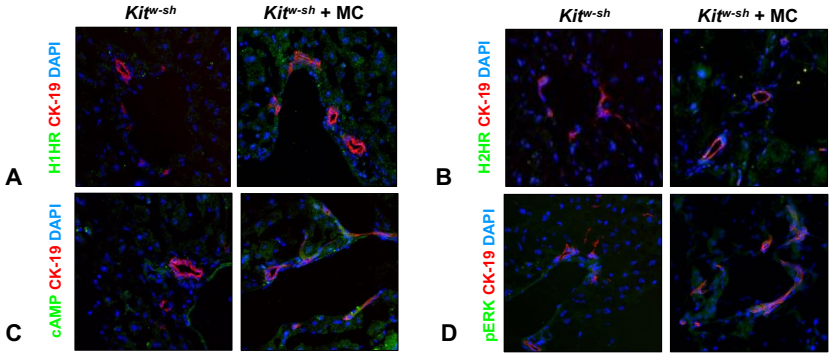

Figure 17, Determination of H1HR, H2HR, and cAMP/pERK Expression Following MC Injection. Evaluation of H1HR, H2HR and cAMP/pERK expression in *Kit*$^{W\text{-}sh}$ mice injected with MCs. (A) H1HR expression is slightly increased in small ducts and peripheral, non-biliary cells following MC injection into *Kit*$^{W\text{-}sh}$ mice when compared to control injected counterparts. (B) H2HR expression is increased *Kit*$^{W\text{-}sh}$ mice injected with MCs. (C) Injection of MCs increases large duct expression of cAMP in *Kit*$^{W\text{-}sh}$ mice. (D) Similarly, MC injection increases pERK expression in large ducts in *Kit*$^{W\text{-}sh}$ mice. Images are 80× magnification.

Loss of MCs Reduces Peribiliary Gland Presence, and Expression of vWF and VEGF

Following BDL in WT mice, there is an increase in the presence of peribiliary glands (marked by black arrows) found in close proximity to large bile ducts (indicated by the yellow arrow) when compared to sham WT mice (Figure 18A). However, in both sham and BDL *Kit*$^{W\text{-}sh}$ mice, there is no visible evidence of peribiliary glands (Figure 18A) compared to BDL WT mice. Further, VEGF-C expression is significantly reduced in BDL *Kit*$^{W\text{-}sh}$ mice compared to BDL WT mice (Figure 18B). Immunofluorescence for vWF

demonstrates an increase in BDL WT mice compared to sham WT mice, and in BDL *Kit*$^{W\text{-}sh}$ mice there is a marked decrease in the expression of vWF compared to BDL WT (Figure 18C). Similarly, vWF gene expression is increased in BDL WT mice compared to WT mice, and in BDL *Kit*$^{W\text{-}sh}$ mice there is a marked decrease in the expression of vWF compared to BDL WT mice (Figure 18D). These data indicate that MCs not only influence the biliary epithelium, but also the peribiliary glands and the vascular bed during BDL-induced liver damage.

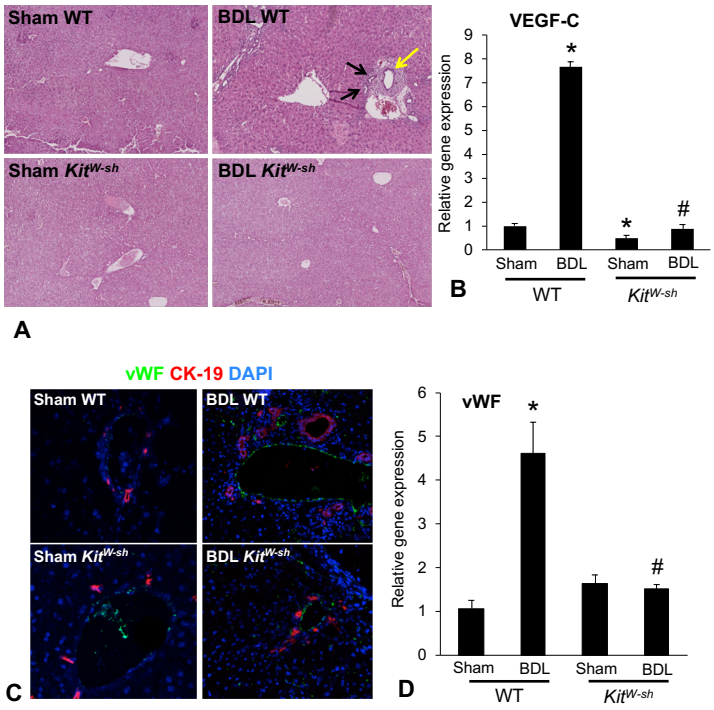

Figure 18, Presence of Peribiliary Glands and Endothelial Cells Following BDL. Evaluation of peribiliary glands and vascular cell presence in WT and *Kit*$^{W\text{-}sh}$ mice subjected to sham or BDL surgery. (A) H&E staining reveals the presence of peribiliary glands in BDL WT mice (black arrows) in close proximity to large bile ducts (yellow arrow), whereas sham WT mice, and sham and BDL *Kit*$^{W\text{-}sh}$ mice have no visible peribiliary glands. (B) VEGF-C expression is increased in total liver from BDL WT mice compared to sham WT mice, which is decreased in BDL *Kit*$^{W\text{-}sh}$ mice. (C) vWF expression (green) is upregulated in BDL WT compared to sham WT mice, whereas vWF is reduced in sham and BDL *Kit*$^{W\text{-}sh}$ mice. (D) vWF gene expression is increased in total liver from BDL WT mice compared to sham WT mice and is reduced in BDL *Kit*$^{W\text{-}sh}$ mice compared to BDL WT mice. Data are expressed as mean ± SEM of 6 experiments for *q*PCR. *p<0.05 versus sham WT mice; #p<0.05 versus BDL WT mice. Images are 10× magnification for H&E and 20× for immunofluorescence.

MC Injection Increases vWF and VEGF Expression in *Kit*$^{W\text{-}sh}$ Mice

There was no significant change in peribiliary gland presence in *Kit*$^{W\text{-}sh}$ mice injected with MCs versus control mice (not shown). The injection of MCs into *Kit*$^{W\text{-}sh}$ mice was able to significantly increase vWF expression and VEGF-C gene expression when compared to vehicle-injected mice (Figure 19A and B).

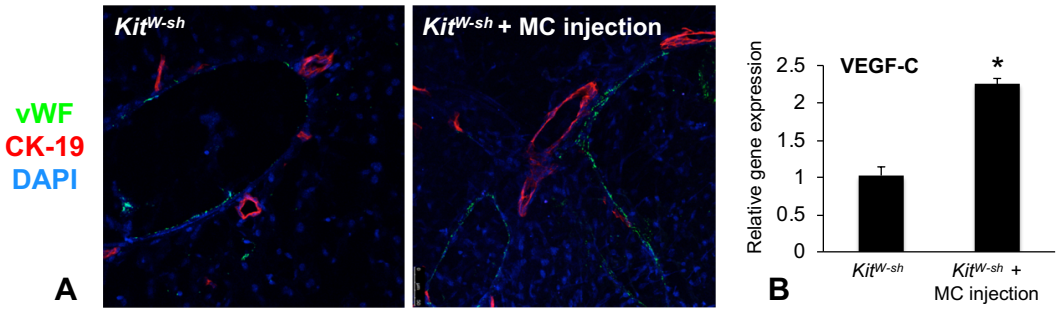

Figure 19, Evaluation of Endothelial Cell Presence and VEGF-C Levels Following MC Injection. Determination of vascular cell presence in *Kit*$^{W\text{-}sh}$ mice injected with MCs or vehicle. (A) vWF expression (green) is upregulated in *Kit*$^{W\text{-}sh}$ mice injected with MCs when compared to vehicle-injected mice. (B) VEGF-C gene expression is increased in total liver from *Kit*$^{W\text{-}sh}$ mice injected with MCs when compared to vehicle-injected mice. *p<0.05 versus *Kit*$^{W\text{-}sh}$ mice. Images are 20× magnification.

H2HR Vivo Morpholino Treatment Ameliorates Hepatic Damage, Inflammation and Necrosis in *Mdr2*$^{-/-}$ Mice

Since we found that (i) MCs primarily regulate large (but not small) biliary proliferation, (ii) large cholangiocytes express H2HR, and (iii) H2HR is predominantly increased in models of cholestasis, we wanted to further evaluate the role of H2HR signaling on large duct damage and subsequent liver injury in the *Mdr2*$^{-/-}$ mouse model of PSC. By H&E staining and serum chemistry, we found that blocking expression of the

H2HR by Vivo Morpholino treatment downregulated hepatic damage and serum levels of γ-GT, a marker of cholangiocyte damage in *Mdr2*$^{-/-}$ mice, when compared to mismatch morpholino controls (Figure 20A and B). Similar to our BDL model, *Mdr2*$^{-/-}$ mice treated with mismatch morpholino had a significant increase in peribiliary gland presence (black arrows) surrounding a large duct (yellow arrow). Peribiliary glands were reduced in *Mdr2*$^{-/-}$ mice treated with H2HR Vivo Morpholino (Figure 20A). Further, inflammation and necrosis were reduced in *Mdr2*$^{-/-}$ mice treated with H2HR Vivo Morpholinos compared to mismatch-treated *Mdr2*$^{-/-}$ mice (Figure 20A and B).

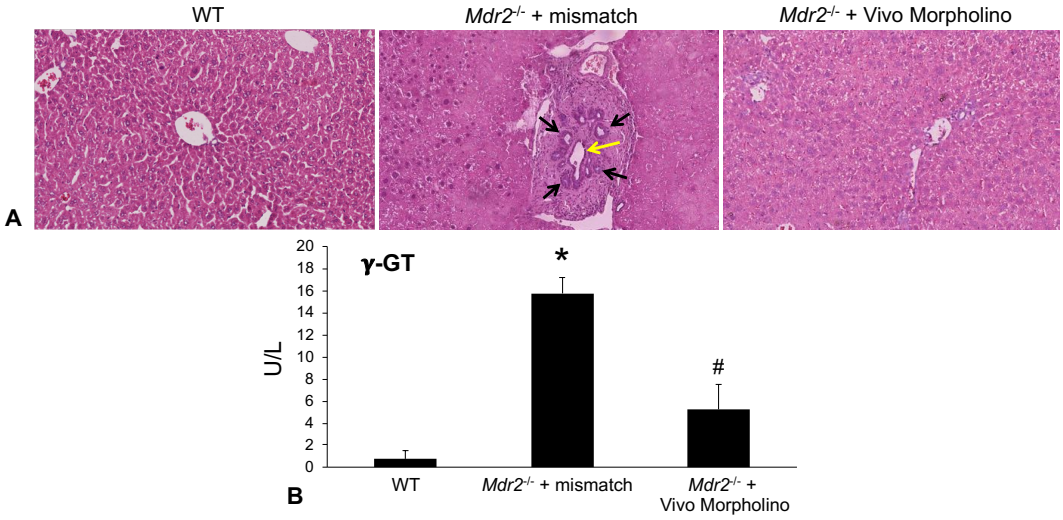

Figure 20, Assessment of Liver Injury and Peribiliary Gland Presence Following H2HR Vivo Morpholino Treatment. Assessment of liver injury in *Mdr2*$^{-/-}$ mice treated with H2HR Vivo Morpholino. (A) H&E staining shows increased portal inflammation, peribiliary fibrosis, large duct damage (yellow arrow) and the presence of peribiliary glands (black arrows) in *Mdr2*$^{-/-}$ mice treated with mismatch morpholinos versus WT mice. H2HR Vivo Morpholino treatment reduced these findings in *Mdr2*$^{-/-}$ mice. (B) Serum levels of γ-GT (marker of biliary damage) are increased in *Mdr2*$^{-/-}$ mice treated with mismatch morpholino versus WT mice, but this is decreased in *Mdr2*$^{-/-}$ mice treated with H2HR Vivo Morpholinos. Data are expressed as mean ± SEM of 4 experiments for EIA. *p<0.05 versus WT; #p<0.05 versus *Mdr2*$^{-/-}$ mice + mismatch. Images are 20× magnification.

MCs and the Histamine/H2HR Signaling Pathway Are Decreased in *Mdr2*$^{-/-}$ Mice Treated with H2HR Vivo Morpholinos

MC infiltration was upregulated in *Mdr2*$^{-/-}$ mice treated with mismatch morpholinos (similar to previous studies (15, 37, 100)), as demonstrated by immunohistochemical assessment of mMCP-1 and *q*PCR for chymase and c-Kit in total liver, when compared to WT mice (Figure 21A-C). However, H2HR Vivo Morpholino treatment decreased MC number and expression of chymase and c-Kit in *Mdr2*$^{-/-}$ mice when compared to the mismatch--treated group (Figure 21A-C).

Similarly, when *Mdr2*$^{-/-}$ mice were treated with mismatch morpholinos, serum histamine secretion significantly increased compared to WT mice; however, treatment with H2HR Vivo Morpholinos decreased histamine secretion in *Mdr2*$^{-/-}$ mice compared to mismatched morpholino treatment (Figure 22A). Additionally, H2HR and cAMP expression were increased in large cholangiocytes in *Mdr2*$^{-/-}$ livers following mismatch morpholino treatment when compared to WT mice, but these parameters were reduced in *Mdr2*$^{-/-}$ mice treated with H2HR Vivo Morpholinos (Figure 22B).

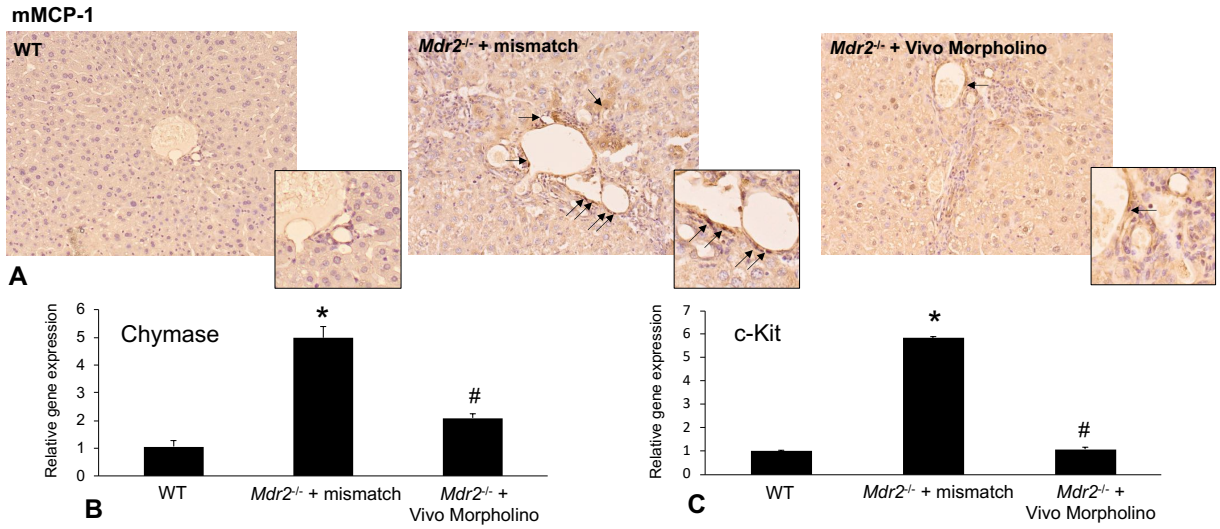

Figure 21, Visualization of Hepatic MCs and MC Marker Expression Following H2HR Vivo Morpholino Treatment. Determination of MC presence in Mdr2$^{-/-}$ mice treated with H2HR vivo morpholinos. (A) By staining for mMCP-1 (MC marker) there was increased MC presence in Mdr2$^{-/-}$ mice treated with mismatch morpholinos as compared to WT mice; however, MC number was reduced in in Mdr2$^{-/-}$ mice treated with H2HR vivo morpholinos. (B) There was increased gene expression of chymase (MC marker) in total liver in mismatch-treated Mdr2$^{-/-}$ mice compared to WT mice, but this was reduced following H2HR vivo morpholino treatment. (C) Similarly, gene expression of c-Kit (MC) in total liver was increased in Mdr2$^{-/-}$ mismatch-treated mice compared to WT mice, but decreased following H2HR vivo morpholino treatment. Data are expressed as mean ± SEM of 4 experiments for *q*PCR. *p<0.05 versus WT; #p<0.05 versus Mdr2$^{-/-}$ mice + mismatch. Images are 20× magnification.

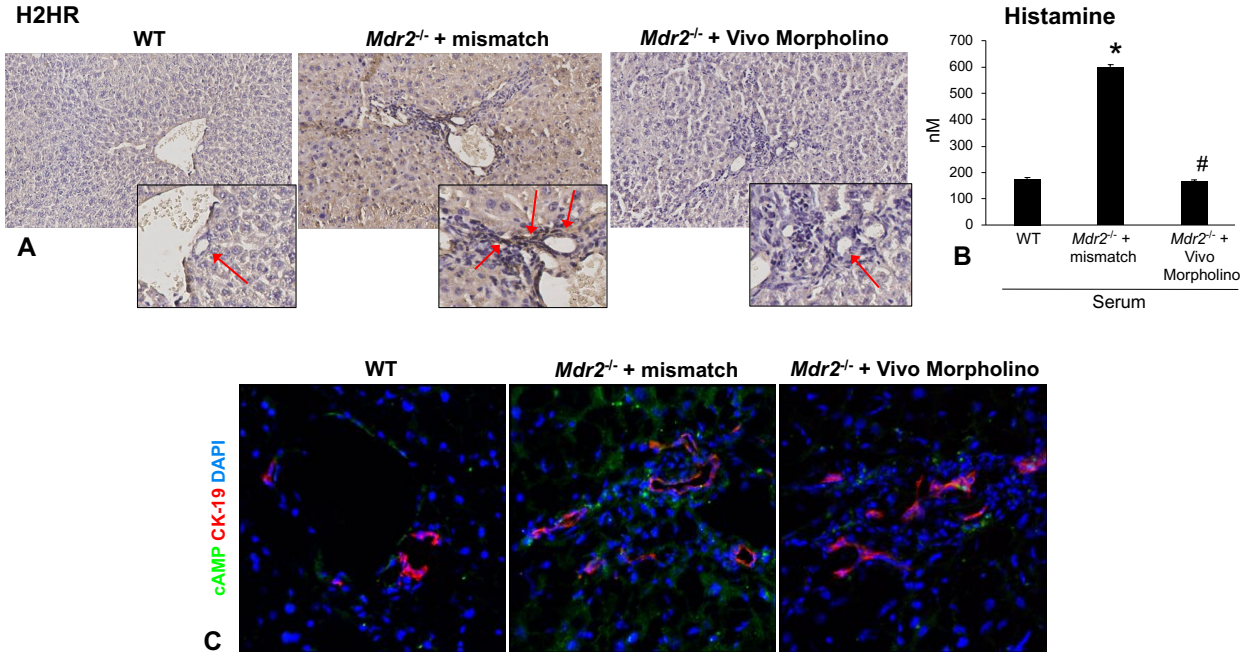

Figure 22, Determination of H2HR and cAMP Expression, and Histamine Secretion Following H2HR Vivo Morpholino Treatment. Assessment of H2HR/cAMP expression and histamine secretion in *Mdr2*$^{-/-}$ mice treated with H2HR Vivo Morpholinos or mismatch. (A) By staining in liver sections, we noted an increase in large duct H2HR expression in *Mdr2*$^{-/-}$ mice treated with mismatch as compared to WT mice; however, this was reduced in *Mdr2*$^{-/-}$ mice treated with H2HR Vivo Morpholinos. (B) There was increased histamine secretion in mismatch-treated *Mdr2*$^{-/-}$ mice compared to WT, but this was reduced following H2HR Vivo Morpholino treatment. (C) Large duct expression of cAMP (downstream of H2HR) was increased in *Mdr2*$^{-/-}$ mismatch mice, but decreased in *Mdr2*$^{-/-}$ mice treated with H2HR Vivo Morpholinos. Data are expressed as mean ± SEM of 4 experiments for EIA. *p<0.05 versus WT; #p<0.05 versus *Mdr2*$^{-/-}$ mice + mismatch. Images for H2HR are 20× magnification and 40× for insets, and 80× for cAMP.

H2HR Vivo Morpholino Treatment Reduces Large IBDM in *Mdr2*$^{-/-}$ Mice

We next evaluated large IBDM and large cholangiocyte proliferation by immunohistochemical assessment of CK-19 and Ki-67 expression. We found that blocking H2HR using Vivo Morpholino treatment decreased large IBDM and large biliary proliferation, respectively, in *Mdr2*$^{-/-}$ mice compared to *Mdr2*$^{-/-}$ mice treated with mismatch morpholino (Figure 23A and B) This compliments our earlier studies demonstrating that large cholangiocytes primarily express H2HR, and that this receptor may preferentially mediate large cholangiocyte proliferation during cholestasis (7, 15).

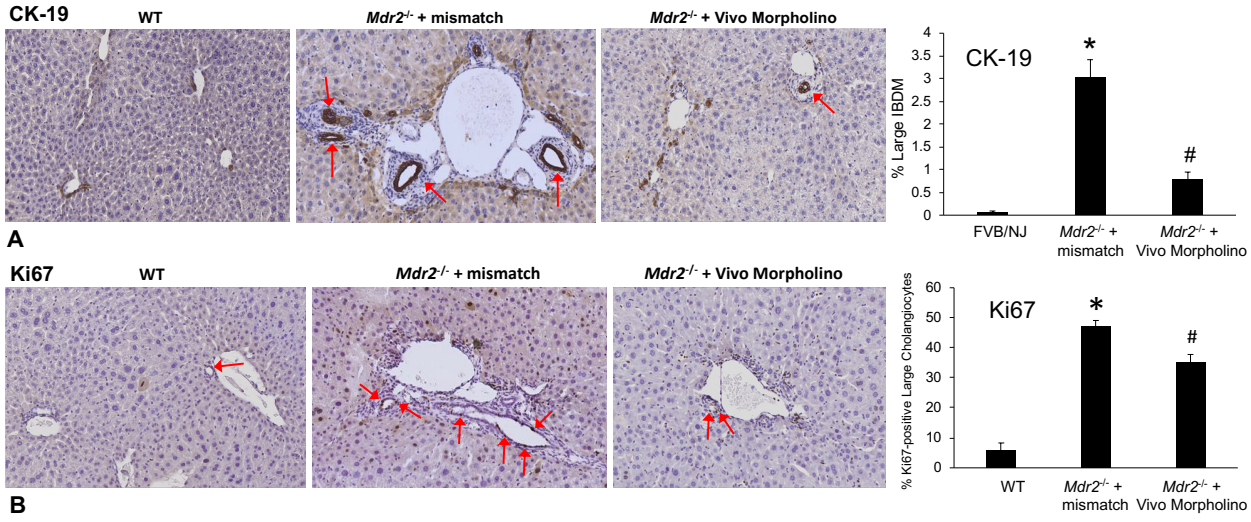

Figure 23, Evaluation of Large IBDM and Large Cholangiocyte Proliferation Following H2HR Vivo Morpholino Treatment. Evaluation of large duct mass and proliferation in *Mdr2*$^{-/-}$ mice treated with H2HR Vivo Morpholinos or mismatch. (A) Immunohistochemistry for CK-19 demonstrated that large duct mass was increased in *Mdr2*$^{-/-}$ mice treated with mismatch as compared to WT mice; however, large duct mass was significantly reduced in *Mdr2*$^{-/-}$ mice treated with H2HR Vivo Morpholino. (B) Similarly, we found a significant increase in large cholangiocyte proliferation, as determined by staining for Ki67, in mismatch-treated *Mdr2*$^{-/-}$ mice compared to WT mice; however, large cholangiocyte proliferation was reduced following H2HR Vivo Morpholino treatment in *Mdr2*$^{-/-}$ mice compared to mismatch treatment. Data are expressed as mean ± SEM of 10 experiments. *p<0.05 versus WT; #p<0.05 versus *Mdr2*$^{-/-}$ mice + mismatch. Images are 20× magnification.

Inflammation, HSC Activation and Liver Fibrosis Are Decreased in *Mdr2*$^{-/-}$ Mice Treated with H2HR Vivo Morpholinos

The presence of Kupffer cells (marked by F4/80 expression) was increased in *Mdr2*$^{-/-}$ mice treated with mismatched morpholinos when compared to WT mice, but this was reduced in *Mdr2*$^{-/-}$ mice treated with H2HR Vivo Morpholinos (Figure 24A). Further, the gene expression of CCL2 and CCL5 increased in total liver of *Mdr2*$^{-/-}$ mice treated with mismatched morpholino when compared to WT mice, but was subsequently reduced in *Mdr2*$^{-/-}$ mice treated with H2HR Vivo Morpholinos (Figure 24B).

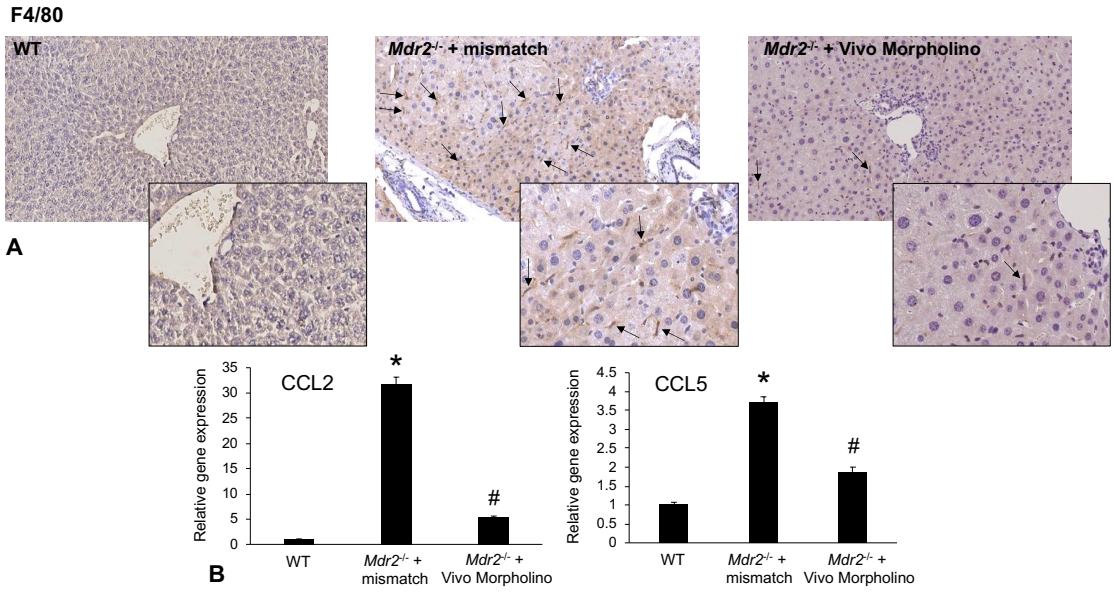

Figure 24, Visualization of Kupffer Cell Number, and CCL2 and CCL5 Expression Following H2HR Vivo Morpholino Treatment. Assessment of Kupffer cell number and liver inflammation in *Mdr2*$^{-/-}$ mice treated with H2HR Vivo Morpholinos or mismatch. (A) Staining for F4/80 (marker of Kupffer cells) showed that Kupffer cell number was increased in *Mdr2*$^{-/-}$ mice treated with mismatch as compared to WT mice, but was decreased following H2HR Vivo Morpholino treatment in *Mdr2*$^{-/-}$ mice. (B) As determined by *q*PCR in total liver, gene expression of CCL2 and CCL5 were significantly increased in *Mdr2*$^{-/-}$ mismatch-treated mice compared to WT mice; however, CCL2 and CCL5 gene expression decreased following H2HR Vivo Morpholino treatment in *Mdr2*$^{-/-}$ mice compared to mismatch treatment. Data are expressed as mean ± SEM of 4 experiments for *q*PCR. *p<0.05 versus WT; #p<0.05 versus *Mdr2*$^{-/-}$ mice + mismatch. Images are 20× magnification, 40× for insets.

Sirius Red staining and hydroxyproline content both demonstrated an increase in collagen deposition in *Mdr2*$^{-/-}$ mice treated with mismatched Vivo Morpholinos that was significantly reduced in *Mdr2*$^{-/-}$ mice treated with H2HR Vivo Morpholinos (Figure 25A and B). Similarly, HSC activation decreased in *Mdr2*$^{-/-}$ mice treated with H2HR Vivo Morpholinos compared to mismatch treatment, as shown by immunofluorescence for SYP-9 (Figure 26A).

A hallmark feature of increased hepatic fibrosis is elevated TGF-β1 expression and secretion. Serum levels of TGF-β1 increased in *Mdr2*$^{-/-}$ mice treated with mismatched Vivo Morpholinos, which was significantly reduced in *Mdr2*$^{-/-}$ mice treated with H2HR Vivo Morpholinos (Figure 26B). In addition, by *q*PCR in isolated large cholangiocytes and immunofluorescence in liver sections, we found that TGF-β1 expression decreases in *Mdr2*$^{-/-}$ mice treated with the H2HR Vivo Morpholinos compared to *Mdr2*$^{-/-}$ mice treated with mismatch Vivo Morpholinos (Figure 26C and D).

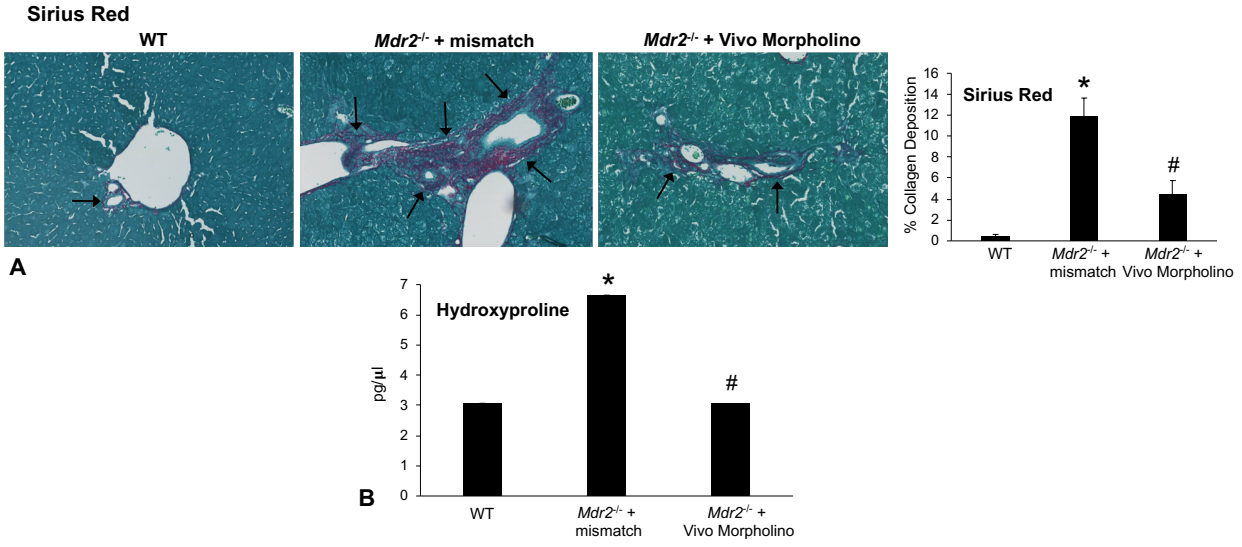

Figure 25, Determination of Liver Fibrosis Following H2HR Vivo Morpholino Treatment. Determination of liver fibrosis in *Mdr2*$^{-/-}$ mice treated with H2HR Vivo Morpholino or mismatch. (A) Sirius Red staining and semi-quantification demonstrated a significant increase in collagen deposition in *Mdr2*$^{-/-}$ mice treated with mismatch as compared to WT mice, but this was decreased following H2HR Vivo Morpholino treatment in *Mdr2*$^{-/-}$ mice as compared to mismatch treatment. (B) In total liver, there was an increase in hydroxyproline content in *Mdr2*$^{-/-}$ mismatch-treated mice compared to WT mice; however, hydroxyproline content was significantly decreased following H2HR Vivo Morpholino treatment in *Mdr2*$^{-/-}$ mice compared to mismatch treatment. Data are expressed as mean ± SEM of 10 experiments for Sirius Red and 4 experiments for hydroxyproline. *p<0.05 versus WT; #p<0.05 versus *Mdr2*$^{-/-}$ mice + mismatch. Images are 20× magnification.

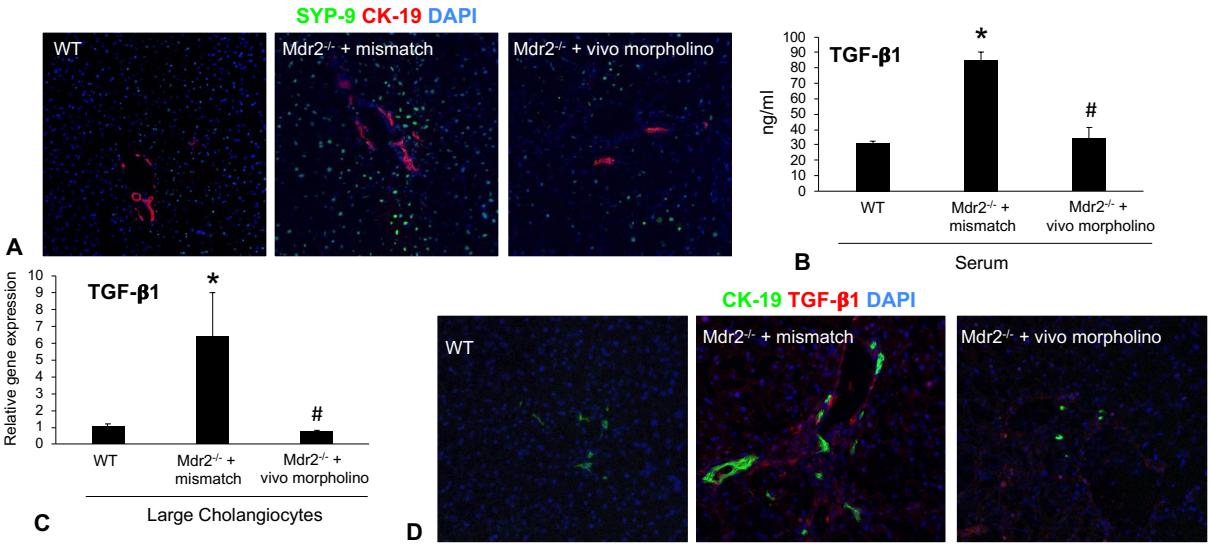

Figure 26, Evaluation of HSC Activation and TGF-β1 Secretion Following H2HR Vivo Morpholino Treatment. Evaluation of HSC activation and TGF-**β**1 levels in *Mdr2*$^{-/-}$ mice treated with H2HR Vivo Morpholinos or mismatch. (A) Immunofluorescence for SYP-9 (green) showed increased HSC activation in *Mdr2*$^{-/-}$ mismatch mice as compared to WT mice, but this was decreased following H2HR Vivo Morpholino treatment. (B) Serum TGF-**β**1 serum levels were increased in *Mdr2*$^{-/-}$ mismatch-treated mice compared to WT mice, but significantly decreased in *Mdr2*$^{-/-}$ mice treated with H2HR Vivo Morpholinos. (C) Gene expression of TGF-**β**1 was increased in large cholangiocytes in *Mdr2*$^{-/-}$ mismatch-treated mice compared to WT mice. H2HR Vivo Morpholino treatment reduced large cholangiocyte TGF-**β**1 gene expression compared to mismatch treatment. (D) Hepatic expression of TGF-**β**1 was increased in *Mdr2*$^{-/-}$ mismatch-treated mice compared to WT mice, but reduced following H2HR Vivo Morpholino treatment. Data are expressed as mean ± SEM of 4 experiments for EIA and 4 experiments for *q*PCR. *p<0.05 versus WT; #p<0.05 versus *Mdr2*$^{-/-}$ mice + mismatch. Images are 20× magnification for SYP-9 and 40× magnification for TGF-**β**1.

Inhibition of H2HR by Vivo Morpholino Treatment Decreases Angiogenesis and Large Cholangiocyte VEGF Expression/Secretion in *Mdr2*$^{-/-}$ Mice

In *Mdr2*$^{-/-}$ mice treated with H2HR Vivo Morpholinos we found a decrease in vWF expression shown by immunofluorescence and *q*PCR in total liver compared to *Mdr2*$^{-/-}$ mice treated with mismatch Vivo Morpholinos (Figure 27A and B). VEGF-A/C gene

expression increased in large cholangiocytes isolated from *Mdr2*$^{-/-}$ mismatch-treated mice was significantly reduced in large cholangiocytes isolated from *Mdr2*$^{-/-}$ mice treated with H2HR Vivo Morpholinos (Figure 27C and D). Finally, VEGF-A secretion was evaluated in large cholangiocyte supernatant and, in *Mdr2*$^{-/-}$ mismatch-treated mice, there was an increase in VEGF-A levels that was decreased in large cholangiocyte supernatant from *Mdr2*$^{-/-}$ mice treated with H2HR Vivo Morpholinos (Figure 27E). These data support our previous work demonstrating that histamine and HRs regulate angiogenesis and VEGF signaling (36, 100).

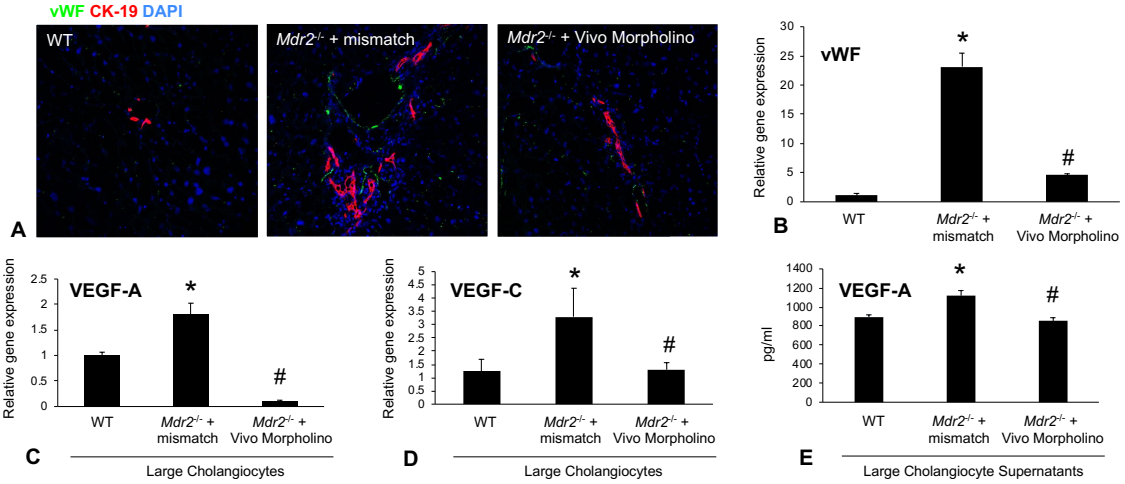

Figure 27, Assessment of Hepatic vWF Expression, Large Cholangiocyte VEGF-A/C Expression and Large Cholangiocyte VEGF-A Secretion Following H2HR Vivo Morpholino Treatment. Measurement of angiogenesis and VEGF expression/secretion in *Mdr2*$^{-/-}$ mice treated with H2HR Vivo Morpholino or mismatch. (A) Immunofluorescence for vWF (green) demonstrated enhanced vWF expression in *Mdr2*$^{-/-}$ mismatch-treated mice as compared to WT mice; however, vWF expression was reduced in H2HR Vivo Morpholino-treated *Mdr2*$^{-/-}$ mice. (B) Additionally, the gene expression of vWF was increased in total liver from *Mdr2*$^{-/-}$ mismatch-treated mice compared to WT mice, but significantly decreased in *Mdr2*$^{-/-}$ H2HR Vivo Morpholino-treated mice. (C) Gene expression of VEGF-A and (D) VEGF-C was increased in large cholangiocytes in *Mdr2*$^{-/-}$ mismatch-treated mice compared to WT mice. H2HR Vivo Morpholino treatment reduced large cholangiocyte gene expression of VEGF-A and VEGF-C compared to mismatch treatment. (E) Similarly, large cholangiocyte secretion of VEGF-A increased in Mdr2$^{-/-}$ mismatch-treated mice compared to WT, but reduced following H2HR Vivo Morpholino treatment. Data are expressed as mean ± SEM of 4 experiments for *q*PCR and 4 experiments for EIA. *p<0.05 versus WT; #p<0.05 versus *Mdr2*$^{-/-}$ mice + mismatch. Images are 20× magnification for SYP-9 and 40× magnification for TGF-**β**1.

In Vitro, MCs Migrate Towards Damaged Large, But Not Small, Cholangiocytes

To evaluate the capacity of MCs to migrate towards injured small and large cholangiocytes, we treated small and large cholangiocytes with LPS *in vitro* prior to placing the damaged cholangiocytes in the lower well of Boyden chambers and loading the top well with MCs. Following 24 hrs of incubation, we found that MCs migrate towards both unstimulated small and large cholangiocytes when compared to control wells containing no cells in the lower well (Figure 28). Interestingly, small cholangiocytes treated with LPS show no change in MC migration when compared to undamaged controls; however, large cholangiocytes treated with LPS significantly increased MC migration when compared to controls (Figure 28). These data confirm our *in vivo* findings that MCs preferentially migrate towards damaged large ducts.

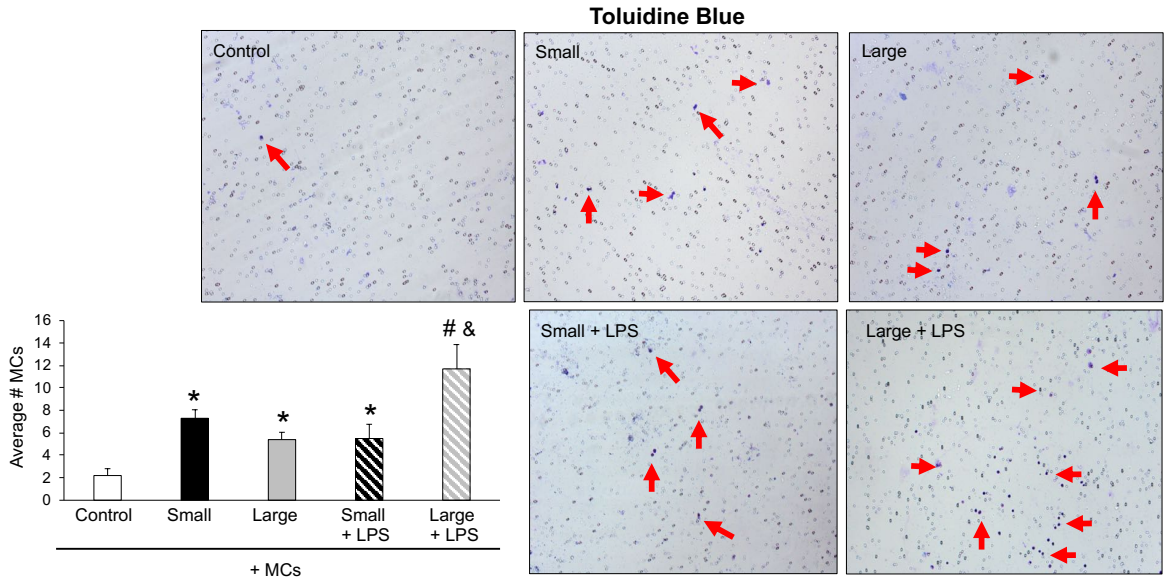

Figure 28, *In Vitro* Determination of MC Migration Towards Small or Large Cholangiocytes Treated with LPS. Assessment of MC migration to small and large cholangiocytes treated with LPS (to induce damage). To evaluate MC migration, we loaded the top well of Boyden chambers with MCs and the bottom chamber with no cells (control), untreated small or large cholangiocytes, or small or large cholangiocytes treated with LPS (100 ng/ml) for 24 hrs. As shown by Toluidine blue staining, MC migration towards untreated small and large cholangiocytes increased compared to control wells containing no cells. However, MC migration increased towards damaged large, but not small, cholangiocytes when compared to untreated counterparts. n=10 pictures evaluated for Toluidine blue staining. *p<0.05 vs control; #p<0.05 vs Large; &p<0.05 vs Small + LPS. Images are 20× magnification.

In Vitro, MCs Promote Large Cholangiocyte Damage and H2HR/cAMP Signaling

Since we have verified that MCs primarily interact with large but not small cholangiocytes, we utilized cultured large cholangiocytes for the remainder of our studies. We next evaluated phenotypic changes in large cholangiocytes that were treated with supernatants from either cultured MCs or MCs pre-treated with the HDC inhibitor, α-Me (to block histamine synthesis in MCs). We noted that large cholangiocytes exposed to supernatants from untreated MCs demonstrated increased proliferation as shown by PCNA immunofluorescence (Figure 29A). Of note, we found that large cholangiocytes treated with supernatants from untreated MCs had an increase in cellular senescence as

demonstrated by p18 expression (Figure 29B). However, both proliferation and senescence were decreased in large cholangiocytes that were treated with supernatants from MC pre-treated with α-Me (Figure 29A and B). We next evaluated HR expression in large cholangiocytes and found that H1HR expression did not significantly change in large cholangiocytes treated with supernatants from control MCs or αMe-treated MCs (Figure 29C). As expected, H2HR expression was significantly upregulated in large cholangiocytes treated with MC supernatants, but this change was not seen in large cholangiocytes treated with supernatants from αMe-treated MCs (Figure 29D). These changes mimic our *in vivo* findings where we see a strong increase in H2HR expression, over H1HR, in large cholangiocytes during cholestasis.

We next examined the downstream effectors of H2HR signaling to determine if MC-derived histamine mediates these changes. We found that both cAMP and pERK expression were increased in large cholangiocytes treated with MC supernatants; however, these findings were significantly reduced in large cholangiocytes treated with supernatants from MCs pre-treated with α-Me (Figure 29E and F). Similarly, large cholangiocytes treated with MC supernatants had increased cellular cAMP levels, which were significantly reduced in large cholangiocytes stimulated with supernatants from MCs pre-treated with α-Me (Figure 30). Our data indicate that MC-derived histamine promotes large cholangiocyte proliferation, senescence and H2HR signaling *in vitro*.

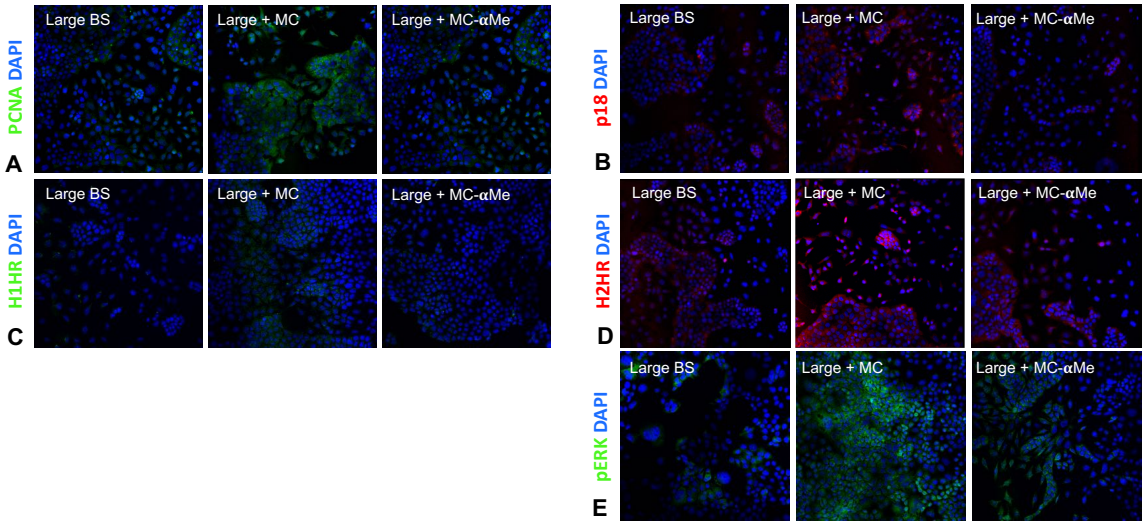

Figure 29, Visualization of Large Cholangiocyte Expression of PCNA, p18, H1HR, H2HR and pERK Following Stimulation with MC Supernatants. Visualization of large cholangiocyte phenotype following treatment with supernatants from MCs and MCs pre-treated with αMe. (A) Large cholangiocytes treated with MC supernatants displayed increased proliferation, as shown by PCNA staining, but this was decreased in large cholangiocytes treated with supernatants from MCs pre-treated with αMe. (B) Interestingly, MC supernatants promoted large cholangiocyte senescence (p18 expression), but this was reduced in large cholangiocytes treated with supernatants from MCs pre-treated with αMe. (C) There was no significant change in H1HR expression following stimulation with MC supernatants or supernatants from MCs pre-treated with αMe. (D) Stimulation with MC supernatants upregulated large cholangiocyte H2HR expression, but this was not seen with supernatants from MCs pre-treated with αMe. (E) Large cholangiocyte pERK (downstream of H2HR/cAMP) expression was enhanced following stimulation with MC supernatants, which was not noted in large cholangiocytes treated with supernatants from MCs pre-treated with αMe. Images are 40× magnification.

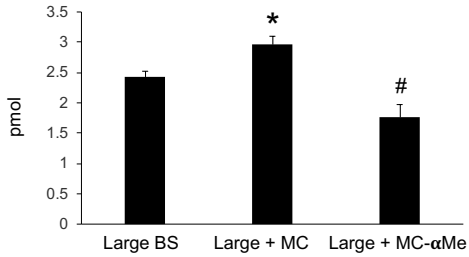

Figure 30, *In Vitro* Measurement of cAMP Levels in Large Cholangiocytes Following Stimulation with MC Supernatants. Measurement of cellular cAMP levels in large cholangiocytes following treatment with supernatants from untreated MCs and MCs treated with αMe. Cellular levels of cAMP, downstream of H2HR activation, were increased in large cholangiocytes treated with untreated-MC supernatants; however, cAMP levels were decreased when large cholangiocytes were treated with αMe-treated MC supernatants. Data are expressed as mean ± SEM of 4 experiments. *$p<0.05$ versus Large BS; #$p<0.05$ versus Large + MC.

CHAPTER IV

CONCLUSIONS*

The main focus of our lab has been to identify the role of MCs and their derived factors on the promotion of damage during various models of liver injury. Our previously published findings have extensively demonstrated that MCs migrate towards bile ducts during models of cholestasis, e.g., PSC and CCA, and inhibition of MC activation in these settings is protective (15, 37, 94, 100). However, the damage seen in these different situations is variable and dependent on the heterogeneity of the biliary tree. Considering the significant differences in small and large cholangiocytes, and their responses to injury, evaluating MC impact on these different subsets of cells is intuitive. PSC is associated with large duct damage and patients with PSC are also at a higher risk for developing large ductal CCA, therefore the investigation of mechanisms regulating large duct damage is clinically warranted.

During cholestatic injury, cholangiocytes hyper-proliferate in order to repair the injured biliary tree. Following BDL, MCs begin to infiltrate the liver beginning at day 2 with hepatic MC number peaking at day 7, and sustained through day 14 (101). Interestingly, MC infiltration does not occur until cholangiocytes have begun to proliferate, suggesting that MC infiltration occurs in response to cholangiocyte damage and supports increased cholangiocyte proliferation following injury. We have also found that MC infiltration is increased even as early as 12 weeks of age and can be seen as late as 52 weeks of age

*Part of this chapter is reprinted with permission from "Bile Duct Ligation-Induced Biliary Hyperplasia, Hepatic Injury, and Fibrosis Are Reduced in Mast Cell-Deficient *Kit*$^{W\text{-}sh}$ Mice" by Hargrove L, Kennedy L, Demieville J, Jones H, Meng F, DeMorrow S, Karstens W, Madeka T, Greene J Jr, Francis H, 2017. *Hepatology*, 65, 1991-2004, Copyright 2017 by John Wiley and Sons.

in the *Mdr2*$^{-/-}$ mouse; however, a time-course study is needed to determine when MCs infiltrate *Mdr2*$^{-/-}$ livers and how MC infiltration correlates with increased bile duct damage.

Our BDL *Kit*$^{W\text{-}sh}$ study is the first to determine the impact of MC deficiency on biliary proliferation following BDL, although it has been shown that MCs promote muscle cell hyperplasia and hypertrophy during eosinophilic esophagitis (127). Furthermore, proliferating cholangiocytes need a consistent supply of growth factors to support their sustained growth. Activated MCs secrete numerous growth factors and pre-formed mediators, such as histamine, VEGF and TGF-β1, that aid in the hyperproliferation of cholangiocytes during cholestasis (15, 36, 79, 80, 100). However, TGF-β1 induces cholangiocyte senescence (12), and we have shown that loss of MCs reduces biliary senescence in a model of NAFLD (9). While MCs promote proliferation, they may inadvertently increase biliary senescence as well. Indeed, one study found that stabilization of MCs attenuated senescence of epididymal white adipose tissue in mice fed a high fat diet (128), and this supports our *in vivo* MC injection studies as well as our *in vitro* analysis.

The interesting take on these findings involves the heterogeneity among cholangiocytes and how they are impacted by MCs and MC-derived mediators. It has been hypothesized that large cholangiocytes are more susceptible to damage, whereas small cholangiocytes are more resistant (4). Following damage, such as in BDL or in *Mdr2*$^{-/-}$ mice, there is an initial upregulation of biliary proliferation but after sustained periods senescent large cholangiocytes become apparent (12). This concept is supported by work presented here; however, we add MCs to the equation by noting that lack of MCs blocks the development of senescence in large cholangiocytes. Further, *in vitro* analysis

determined that blocking MC-derived histamine synthesis and/or release blocks the development of large cholangiocyte senescence. However, it is unclear if histamine signaling directly mediates large cholangiocyte senescence or if it is an indirect effect.

We have repeatedly demonstrated that histamine is a growth promoting factor for cholangiocytes (7, 9, 109), and others have found histamine to be pro-inflammatory (114, 129); therefore, it is possible that large cholangiocytes, which are continually exposed to MC-derived histamine, become highly inflammatory and secrete various cytokines that induce senescence in other neighboring large cholangiocytes. This concept is supported by work wherein large cholangiocyte-derived extracellular vesicles induce inflammatory responses in other large cholangiocytes *in vitro* (10). While cholangiocytes can be categorized into small and large populations, these sub-populations can be even further divided based on cell phenotype. This complex signaling mechanism requires further investigation to fully understand how a sub-population of cholangiocytes can have an even further degree of heterogeneity.

MCs do not infiltrate the liver until bile duct number begins to increase; therefore, proliferating cholangiocytes, that have entered a neuroendocrine phenotype, potentially release factors that promote the migration of MCs to peribiliary areas. It has been demonstrated that there is increased cholangiocyte expression of SCF during human PSC (102), and we have found that SCF secreted from CCA cells induces MC migration through binding with c-Kit (94). During cholestasis, cholangiocytes have increased expression of sphingosine-1-phosphate and TGF-β1 that are known to be strong chemoattractants for MCs (85, 130, 131). Additionally, we found that damaged large cholangiocytes (induced by LPS stimulation *in vitro*) increased MC migration that was not

induced by damaged small cholangiocytes. Differences in secreted factors between damaged small and large cholangiocytes may account for the variation in MC migration. For example, sphingosine-1-phosphate is predominantly found on large instead of small cholangiocytes during bile acid-mediated cholestatic injury (130). Indeed, bioinformatic analysis has shown that large cholangiocytes display increased immune/inflammatory responses (132), and these transcriptional differences may impact MC migration toward small versus large ducts.

Kupffer cells mediate inflammatory changes in the liver during injury (23, 126). Our data indicate that increased MC presence increases Kupffer cell number; however, little work has been done to evaluate the potential signaling mechanisms between these two cell types. It has been shown that MC and Kupffer cell number simultaneously increase during hepatocellular carcinoma (HCC) progression (81), but interaction between the two cell types was not determined. It has been shown that MC-derived IL-1β promotes skin inflammation during cryopyrin-associated periodic syndromes (133). As well, cultured human MCs secrete IL-6 (134), and isolated human intestinal MCs express TNF-α (80). IL-1β, IL-6 and TNF-α promote Kupffer cell pro-inflammatory activities; therefore, MCs may play a direct role in Kupffer cell activation during cholestasis. In support of this, we have found *in vitro* that cultured MC supernatants promote Kupffer cell activation and inflammation (Kennedy and Francis, unpublished observations 2018). While MCs may mediate Kupffer cells directly there may be an unstudied role for MC mediation of large cholangiocytes that in turn affects Kupffer cell activation. However, it is not known if large cholangiocytes, small cholangiocytes or both mediate Kupffer cell activation and the recruitment of blood-derived monocytes. Considering that large cholangiocytes have a

higher capacity for immune and inflammatory responses based on transcriptomic analysis, this subset of cholangiocytes may have a more prominent role in the pro-inflammatory activation of Kupffer cells and the infiltration of macrophages (132). However, it has been shown that human PSC cholangiocytes have increased NFκB signaling that promotes the expression of cytokines and chemokines (135), and these factors may mediate Kupffer cell activation and the inflammatory response. Additionally, whether MCs promote Kupffer cell activation remains unknown. It is apparent that more research is needed to understand (i) how MCs may promote Kupffer cell activation and (ii) how MC interaction with cholangiocytes may mediate inflammatory properties in Kupffer cells.

The role of MCs during fibrogenesis remains controversial. Studies have demonstrated that (i) MCs promote tissue fibrosis; (ii) loss of MCs induces fibrosis leading to a worsening condition and (iii) MCs play no real role in tissue fibrosis. A study using MC-deficient rats found vigorous interstitial fibrosis in the kidney compared to control animals suggesting that, in this model, MCs are beneficial to the fibrotic process (136). In support of our study, it has been demonstrated that MCs promote and drive cardiac fibrosis, and MC-deficient mice are protected from this event (137). In contrast to our work, another study found that MCs have no consequence on the development of liver fibrosis in rats and mice subjected to BDL (138); whereas, our present studies indicate that MC introduction induces robust hepatic fibrosis, and there is decreased fibrotic progression in BDL $Kit^{W\text{-}sh}$ compared to the BDL WT. However, their study involved 21-day BDL; therefore, the reaction of the biliary tree and infiltration of MCs during early events of fibrosis were not evaluated (138). In contrast, our study evaluated

BDL-induced damage no later than 7 days when the biliary tree has been shown to be fully reactive to damage and MC infiltration peaks (101). Another obvious difference is the rodent model of MC deficiency used. The other authors chose *Ws/Ws* rats and male WBB6F$_1$-$^{+/+}$ and *W/W^v* mice, whereas we employed *Kit$^{W\text{-}sh}$* mice that have a different phenotype from these models.

It has not been determined whether large or small cholangiocytes mediate HSC activation and subsequent liver fibrosis. In *Mdr2$^{-/-}$* mice (that present with increased large duct damage) there is increased biliary senescence driven by B-cell lymphoma-extra large (Bcl-xL) expression (108). Inhibition of Bcl-xL significantly decreased cholangiocyte senescence, thus reducing fibroblast activation and liver fibrosis (108). Understanding the differential roles of heterogenous cholangiocytes on the fibrogenic process will be a necessary step in understanding how to treat and monitor different cholangiopathies.

One prominent driver of collagen production in HSCs and a contributor to fibrosis is TGF-β1, which is found within MCs and can be released upon activation. TGF-β1 perpetuates HSC transformation into myofibroblasts, thus inducing fibrosis during disease. We found that ablation of MCs significantly reduces BDL-induced TGF-β1 expression and secretion. In addition, TGF-β1 levels were increased in *Kit$^{W\text{-}sh}$* mice injected with cultured MCs, supporting the concept that MCs are an important source of TGF-β1 during fibrosis progression. Supporting this is the observation that histamine or angiotensin released from MCs induces secretion of TGF-β1 from fibroblasts that, in turn, increases collagen synthesis and pulmonary fibrosis induction. When MCs were absent, these events were inhibited (139). Furthermore, implanted MCs (from WT mice) into MC-deficient mice increases angiogenesis and cardiac function via augmented fibroblast

activity and transformation that was TGF-β1-dependent (140), again pinpointing MC-regulated TGF-β1 as a key player in fibrosis. The full contribution of MCs to liver fibrosis is not completely defined; however, we present strong data herein showing that MCs play a critical and detrimental role in hepatic fibrosis through TGF-β1.

MCs release numerous factors, but a prominent component of MCs is histamine, which has been recognized now to be more than just a mediator of allergic events (79). We have demonstrated in numerous studies that histamine is a trophic, growth-promoting factor that induces biliary hyperplasia, hepatic fibrosis and CCA progression (7, 94, 100, 109, 110). Cholangiocytes secrete minimal amounts of histamine and are able, through autocrine signaling, to regulate CCA growth (141); however, MCs are the major producers of histamine in the body. Stabilization of MCs using cromolyn sodium decreases biliary hyperplasia, fibrosis and CCA growth, pinpointing MC-derived mediators as a culprit in various cholangiopathies (15, 37, 94, 100). In our current study, we measured histamine secretion and H1/H2 HR expression. As expected, all of these factors were upregulated in BDL WT and *Mdr2*$^{-/-}$ mice, but reduced in BDL *Kit*$^{W\text{-}sh}$ mice and *Mdr2*$^{-/-}$ mice treated with H2HR Vivo Morpholinos. These findings further suggest that histamine itself, and histamine receptor signaling, are drivers of biliary hyperplasia and hepatic fibrosis. Histamine signaling through H2HR on large cholangiocytes may drive biliary and liver damage during BDL and in the *Mdr2*$^{-/-}$ mouse model of PSC. In support of this, our lab has previously shown that normal rats treated with an H2HR agonist have increased large cholangiocyte proliferation mediated by cAMP-dependent signaling mechanisms (7). Furthermore, while our mice are MC-deficient, they still receive histidine in their standard chow, and since cholangiocytes secrete small amounts of histamine this may account for

the minimal amount of histamine found in the serum and is consistent with other studies using MC-deficient models or HDC-deficient mice (109).

Besides being a growth-promoting factor, histamine regulates other factors including VEGF during BDL-induced injury and in *Mdr2*$^{-/-}$ mice (100, 109, 110). The peribiliary plexus is a dynamic vascular structure that supports the nutritional needs of the biliary tree and provides the largest source of VEGF in the liver, although cholangiocytes secrete VEGF and express VEGF-R2 and VEGF-R3. MCs also express VEGF receptors and produce VEGF when activated (52, 142). In melanoma, activation of MCs by IgE induces VEGF release that promotes tumor growth (52). In our study we found that BDL *Kit*$^{W\text{-}sh}$ mice and *Mdr2*$^{-/-}$ mice treated with H2HR Vivo Morpholino have lower levels of VEGF-C and further, the vascular bed is altered in these mice as shown by decreased expression of vWF. *Kit*$^{W\text{-}sh}$ mice injected with MCs had increased VEGF-C expression as well as an increase in endothelial cell presence as shown by an increase in total vWF expression. Ghosh et al. found no difference in angiogenic signaling in the MC-deficient WBB6F1-W/W(V) mice compared to controls following implantation of cotton threading to induce granulation tissue formation; however, HDC knockout mice displayed marked alterations in angiogenic signaling (143). Our study demonstrates no significant difference in vascular remodeling between sham WT and sham *Kit*$^{W\text{-}sh}$ mice implying that the effect of MCs is enhanced during pathological conditions. These findings demonstrate that there is a significant loss of biliary reaction in MC-deficient mice that alters the vascular bed, as demonstrated by reduced vWF expression. Since vWF is expressed by endothelial cells, we believe there may be crosstalk between MCs, cholangiocyte and endothelial cells, but more work is necessary to understand exactly how the endothelial cells are impacted. It

is important to note that the peribiliary vascular plexus is primarily found surrounding the large ducts but becomes smaller and more sparse when extended towards the small ducts of the intrahepatic biliary network (53). When large ducts show enhanced inflammation, such as during hepatolithiasis, PSC and extrahepatic biliary obstruction, the vessels increase in number, and during later stages of disease the vessels further increase in number and become dilated (53). However, it has been observed in PSC patients with little bile duct injury that the duct/vessel ratio is near normal (144). There is a delicate balance between large biliary growth and increased vessel number/size that seems to mediate disease progression, and this is supported by our work using H2HR Vivo Morpholinos. It is apparent that vessel growth is secondary to increased bile duct number, but in turn, the bile ducts need the vascular plexus to maintain their growth. Changes in the peribiliary vascular plexus during cholestasis may be directly mediated by MCs, but may also occur indirectly by MCs promoting large cholangiocyte proliferation, which signals to the vascular plexus to increase growth.

In support of the concept that MCs can influence peribiliary gland development, a study examining mammary glands in *Kit*$^{W\text{-}sh}$ mice found that the development of glands, but not their function, was altered compared to WT counterparts (145). These mice were still able to lactate and their mammary glands functioned properly even though the mammary glands were significantly altered during development. The changes demonstrated in our current study regarding IBDM and biliary proliferation coupled with the presence or absence of peribiliary glands suggests that the peribiliary glands are not the sole source of proliferating cholangiocytes. This is supported by numerous studies demonstrating that other factors including secretin, serotonin and VEGF are secreted

from cholangiocytes, which can subsequently influence biliary proliferation in both normal and damaged states (8, 51, 107). However, it is important to note that the peribiliary glands are preferentially located around the large bile ducts (19). These structures contain seromucinous acini and may be a potential stem cell niche for the maintenance of the large ducts of the biliary tree, with the small ducts having their own stem cell population termed hepatic progenitor cells (17, 19, 146). Considering these glands reside near large ducts, and activate in response to substantial damage, it is important to note that inhibition of large cholangiocyte H2HR by Vivo Morpholino treatment in *Mdr2*$^{-/-}$ mice reduced peribiliary gland presence, further signifying the close interaction between large ducts and peribiliary glands during injury. Patients with PSC have increased peribiliary gland hyperplasia that is coupled with progressive biliary fibrosis, and expansion of the peribiliary glands correlated with enhanced stem cell number in these glands (17). One day following BDL there is enhanced expression of stem/progenitor markers in the peribiliary glands along with enhanced proliferation of these biliary stem cells (18). The current hypothesis is that these proliferating biliary stem cells enter a transit-amplifying state and undergo differentiation to become large cholangiocytes, thus restoring the large cholangiocyte population (that underwent senescence or apoptosis induced by damage) or increasing large cholangiocyte number to support the growing biliary tree (17, 18). Since MCs begin to migrate to the liver 2 days following BDL, but peribiliary gland presence is noted 1 day following BDL, the increased stem/progenitor cell proliferation and differentiation may promote the infiltration of MCs. Furthermore, in *Kit*$^{W\text{-}sh}$ mice, we see an increase in small duct mass with a decrease in large duct mass compared to WT mice, and this finding is more prominent in BDL *Kit*$^{W\text{-}sh}$ mice compared to BDL WT mice.

MCs may support the needs of the peribiliary glands and loss of MCs reduces their proliferative capacity, thereby reducing the ability of large ducts to repair themselves, leading to compensatory growth of the small ducts to help alleviate damage.

Clinically speaking, the depletion of MCs throughout the whole body is not likely to be a healthy scenario as they are necessary during wound healing, but mechanisms to block MCs and the mediators they release may rescue the liver from biliary damage, hepatic fibrosis and vascular bed alteration. Cromolyn sodium is one such drug that targets MC activation, and treatment with cromolyn sodium inhibits biliary hyperplasia and hepatic fibrosis (37, 100). However, there are other factors to consider, as we have described in our study, including TGF-β1 and VEGF. Potential candidates for therapy might include drugs to target and inhibit MC migration (SCF inhibitors) in conjunction with compounds that block VEGF or TGF-β1 release from MCs. Further, microRNAs are being investigated as potential mechanisms to regulate MC activation. For example, miR-223 targets insulin-like growth factor 1 receptor (IGF-1R) in MCs, promoting degranulation and decreasing the PI3K/Akt pathway (147). However, looking downstream of MC activation, blocking histamine signaling (released by MCs and interacting with cholangiocytes) may be a second avenue for the treatment of cholangiopathies. Our previously published work as well as this study identify a significant increase in biliary H2HR in BDL mice, *Mdr2*$^{-/-}$ mice and human PSC (15). We have also found that treatment with the an over-the-counter H2HR antagonist, ranitidine, significantly reduced biliary hyperplasia, liver fibrosis and CCA progression (15). Others have found that ranitidine treatment for gastroesophageal reflux disease in infants decreased symptom score, and was deemed safe for treatment (148). Furthermore, ranitidine treatment shows a strong

antioxidant and protective effect in mice treated with CCl_4 to induce hepatic damage (149). Interestingly, this study found that ranitidine had the strongest effect over the other H2HR antagonists, cimetidine and famotidine (149). However, these publications did not delve into the specific hepatic cell types influenced by H2HR antagonism. Based on our findings that (i) HRs are prominently expressed by cholangiocytes versus other liver cells types and (ii) that H2HR is only increased in large cholangiocytes during models of cholestasis, it is plausible that liver damage is directly mediated by large cholangiocyte H2HR signaling. However, H2HR antagonists may also work to decrease MC migration and activation to the liver, since MCs express this receptor as well. Further studies are necessary to identify the most efficacious H2HR antagonist for the treatment of cholestatic diseases, the specific cell types influenced by H2HR antagonist treatment and whether targeting specific HRs is necessary for the treatment of different liver diseases (i.e. large duct PSC, small duct PSC and PBC).

In conclusion, we have shown that MCs are prominent regulators of biliary hyperplasia, hepatic fibrosis and vascular bed dysfunction demonstrated by the BDL model, through direct injection of MCs into deficient mice and treatment of *Mdr2*$^{-/-}$ mice with H2HR vivo-morpholino. Our studies reveal a synergistic interplay between MCs, cholangiocytes and HSCs, demonstrating the importance of cellular paracrine signaling during disease progression. Since MCs that infiltrate the liver following damage are not resident liver cells, inhibition or knockdown of MCs or MC components are likely therapeutic approaches for patients suffering from cholangiopathies. Furthermore, MCs have a significant impact on large cholangiocyte damage and function during cholestatic injury mediated by H2HR/cAMP/pERK signaling, and modulation of this signaling

mechanism via H2HR antagonist treatment may be a second therapeutic option for patients suffering from large duct damage. Our study warrants the future investigation of modulation of MCs, as well as large cholangiocyte H2HR signaling during cholangiopathies and hepatic fibrosis.

REFERENCES

1. Trefts E, Gannon M, Wasserman DH. The liver. Curr Biol 2017;27:R1147-R1151.

2. Alpini G, Glaser SS, Ueno Y, Pham L, Podila PV, Caligiuri A, LeSage G, et al. Heterogeneity of the proliferative capacity of rat cholangiocytes after bile duct ligation. Am J Physiol 1998;274:G767-775.

3. Glaser S, Wang M, Ueno Y, Venter J, Wang K, Chen H, Alpini G, et al. Differential transcriptional characteristics of small and large biliary epithelial cells derived from small and large bile ducts. Am J Physiol Gastrointest Liver Physiol 2010;299:G769-777.

4. Glaser SS, Gaudio E, Rao A, Pierce LM, Onori P, Franchitto A, Francis HL, et al. Morphological and functional heterogeneity of the mouse intrahepatic biliary epithelium. Lab Invest 2009;89:456-469.

5. Tabibian JH, Masyuk AI, Masyuk TV, O'Hara SP, LaRusso NF. Physiology of cholangiocytes. Compr Physiol 2013;3:541-565.

6. Gaudio E, Barbaro B, Alvaro D, Glaser S, Francis H, Franchitto A, Onori P, et al. Administration of r-VEGF-A prevents hepatic artery ligation-induced bile duct damage in bile duct ligated rats. Am J Physiol Gastrointest Liver Physiol 2006;291:G307-317.

7. Francis HL, Demorrow S, Franchitto A, Venter JK, Mancinelli RA, White MA, Meng F, et al. Histamine stimulates the proliferation of small and large cholangiocytes by activation of both IP3/Ca2+ and cAMP-dependent signaling mechanisms. Lab Invest 2012;92:282-294.

8. Glaser S, Meng F, Han Y, Onori P, Chow BK, Francis H, Venter J, et al. Secretin stimulates biliary cell proliferation by regulating expression of microRNA 125b and microRNA let7a in mice. Gastroenterology 2014;146:1795-1808 e1712.

9. Kennedy L, Hargrove L, Demieville J, Bailey JM, Dar W, Polireddy K, Chen Q, et al. Knockout of l-Histidine Decarboxylase Prevents Cholangiocyte Damage and Hepatic Fibrosis in Mice Subjected to High-Fat Diet Feeding via Disrupted Histamine/Leptin Signaling. Am J Pathol 2018;188:600-615.

10. Sato K, Meng F, Venter J, Giang T, Glaser S, Alpini G. The role of the secretin/secretin receptor axis in inflammatory cholangiocyte communication via extracellular vesicles. Sci Rep 2017;7:11183.

11. Wan Y, Meng F, Wu N, Zhou T, Venter J, Francis H, Kennedy L, et al. Substance P increases liver fibrosis by differential changes in senescence of cholangiocytes and hepatic stellate cells. Hepatology 2017;66:528-541.

12. Wu N, Meng F, Zhou T, Venter J, Giang TK, Kyritsi K, Wu C, et al. The Secretin/Secretin Receptor Axis Modulates Ductular Reaction and Liver Fibrosis through Changes in Transforming Growth Factor-beta1-Mediated Biliary Senescence. Am J Pathol 2018;188:2264-2280.

13. Francis H, Glaser S, Demorrow S, Gaudio E, Ueno Y, Venter J, Dostal D, et al. Small mouse cholangiocytes proliferate in response to H1 histamine receptor stimulation by activation of the IP3/CaMK I/CREB pathway. Am J Physiol Cell Physiol 2008;295:C499-513.

14. Mancinelli R, Franchitto A, Gaudio E, Onori P, Glaser S, Francis H, Venter J, et al. After damage of large bile ducts by gamma-aminobutyric acid, small ducts replenish the biliary tree by amplification of calcium-dependent signaling and de novo acquisition of large cholangiocyte phenotypes. Am J Pathol 2010;176:1790-1800.

15. Kennedy L, Hargrove L, Demieville J, Karstens W, Jones H, DeMorrow S, Meng F, et al. Blocking H1/H2 histamine receptors inhibits damage/fibrosis in Mdr2(-/-) mice and human cholangiocarcinoma tumorigenesis. Hepatology 2018.

16. Francis H, Franchitto A, Ueno Y, Glaser S, DeMorrow S, Venter J, Gaudio E, et al. H3 histamine receptor agonist inhibits biliary growth of BDL rats by downregulation of the cAMP-dependent PKA/ERK1/2/ELK-1 pathway. Lab Invest 2007;87:473-487.

17. Carpino G, Cardinale V, Renzi A, Hov JR, Berloco PB, Rossi M, Karlsen TH, et al. Activation of biliary tree stem cells within peribiliary glands in primary sclerosing cholangitis. J Hepatol 2015;63:1220-1228.

18. DiPaola F, Shivakumar P, Pfister J, Walters S, Sabla G, Bezerra JA. Identification of intramural epithelial networks linked to peribiliary glands that express progenitor cell markers and proliferate after injury in mice. Hepatology 2013;58:1486-1496.

19. Nakanuma Y, Katayanagi K, Terada T, Saito K. Intrahepatic peribiliary glands of humans. I. Anatomy, development and presumed functions. J Gastroenterol Hepatol 1994;9:75-79.

20. Gao B, Jeong WI, Tian Z. Liver: An organ with predominant innate immunity. Hepatology 2008;47:729-736.

21. Smedsrod B, De Bleser PJ, Braet F, Lovisetti P, Vanderkerken K, Wisse E, Geerts A. Cell biology of liver endothelial and Kupffer cells. Gut 1994;35:1509-1516.

22. MacPhee PJ, Schmidt EE, Groom AC. Evidence for Kupffer cell migration along liver sinusoids, from high-resolution in vivo microscopy. Am J Physiol 1992;263:G17-23.

23. Guicciardi ME, Trussoni CE, Krishnan A, Bronk SF, Lorenzo Pisarello MJ, O'Hara SP, Splinter PL, et al. Macrophages contribute to the pathogenesis of sclerosing cholangitis in mice. J Hepatol 2018;69:676-686.

24. Laskin DL, Sunil VR, Gardner CR, Laskin JD. Macrophages and tissue injury: agents of defense or destruction? Annu Rev Pharmacol Toxicol 2011;51:267-288.

25. Sica A, Mantovani A. Macrophage plasticity and polarization: in vivo veritas. J Clin Invest 2012;122:787-795.

26. Fujita T, Soontrapa K, Ito Y, Iwaisako K, Moniaga CS, Asagiri M, Majima M, et al. Hepatic stellate cells relay inflammation signaling from sinusoids to parenchyma in mouse models of immune-mediated hepatitis. Hepatology 2016;63:1325-1339.

27. Stewart RK, Dangi A, Huang C, Murase N, Kimura S, Stolz DB, Wilson GC, et al. A novel mouse model of depletion of stellate cells clarifies their role in ischemia/reperfusion- and endotoxin-induced acute liver injury. J Hepatol 2014;60:298-305.

28. Terada M, Horisawa K, Miura S, Takashima Y, Ohkawa Y, Sekiya S, Matsuda-Ito K, et al. Kupffer cells induce Notch-mediated hepatocyte conversion in a common mouse model of intrahepatic cholangiocarcinoma. Sci Rep 2016;6:34691.

29. Rose KA, Holman NS, Green AM, Andersen ME, LeCluyse EL. Co-culture of Hepatocytes and Kupffer Cells as an In Vitro Model of Inflammation and Drug-Induced Hepatotoxicity. J Pharm Sci 2016;105:950-964.

30. Su L, Li N, Tang H, Lou Z, Chong X, Zhang C, Su J, et al. Kupffer cell-derived TNF-alpha promotes hepatocytes to produce CXCL1 and mobilize neutrophils in response to necrotic cells. Cell Death Dis 2018;9:323.

31. Ellis EL, Mann DA. Clinical evidence for the regression of liver fibrosis. J Hepatol 2012;56:1171-1180.

32. Perepelyuk M, Terajima M, Wang AY, Georges PC, Janmey PA, Yamauchi M, Wells RG. Hepatic stellate cells and portal fibroblasts are the major cellular sources of collagens and lysyl oxidases in normal liver and early after injury. Am J Physiol Gastrointest Liver Physiol 2013;304:G605-614.

33. Puche JE, Saiman Y, Friedman SL. Hepatic stellate cells and liver fibrosis. Compr Physiol 2013;3:1473-1492.

34. Krizhanovsky V, Yon M, Dickins RA, Hearn S, Simon J, Miething C, Yee H, et al. Senescence of activated stellate cells limits liver fibrosis. Cell 2008;134:657-667.

35. Parenti P, Villa M, Hanozet GM. Kinetics of leucine transport in brush border membrane vesicles from lepidopteran larvae midgut. J Biol Chem 1992;267:15391-15397.

36. Hargrove L, Kennedy L, Demieville J, Jones H, Meng F, DeMorrow S, Karstens W, et al. Bile duct ligation-induced biliary hyperplasia, hepatic injury, and fibrosis are reduced in mast cell-deficient Kit(W-sh) mice. Hepatology 2017;65:1991-2004.

37. Kennedy LL, Hargrove LA, Graf AB, Francis TC, Hodges KM, Nguyen QP, Ueno Y, et al. Inhibition of mast cell-derived histamine secretion by cromolyn sodium treatment decreases biliary hyperplasia in cholestatic rodents. Lab Invest 2014;94:1406-1418.

38. Semenza GL. Hypoxia-inducible factors in physiology and medicine. Cell 2012;148:399-408.

39. Carmeliet P, Jain RK. Molecular mechanisms and clinical applications of angiogenesis. Nature 2011;473:298-307.

40. Fernandez M, Semela D, Bruix J, Colle I, Pinzani M, Bosch J. Angiogenesis in liver disease. J Hepatol 2009;50:604-620.

41. Gabriel A, Kukla M, Wilk M, Liszka L, Petelenz M, Musialik J. Angiogenesis in chronic hepatitis C is associated with inflammatory activity grade and fibrosis stage. Pathol Res Pract 2009;205:758-764.

42. Ciupinska-Kajor M, Hartleb M, Kajor M, Kukla M, Wylezol M, Lange D, Liszka L. Hepatic angiogenesis and fibrosis are common features in morbidly obese patients. Hepatol Int 2013;7:233-240.

43. Bruno A, Pagani A, Pulze L, Albini A, Dallaglio K, Noonan DM, Mortara L. Orchestration of angiogenesis by immune cells. Front Oncol 2014;4:131.

44. Novo E, Cannito S, Paternostro C, Bocca C, Miglietta A, Parola M. Cellular and molecular mechanisms in liver fibrogenesis. Arch Biochem Biophys 2014;548:20-37.

45. Tecchio C, Cassatella MA. Neutrophil-derived cytokines involved in physiological and pathological angiogenesis. Chem Immunol Allergy 2014;99:123-137.

46. Simpson KJ, Henderson NC, Bone-Larson CL, Lukacs NW, Hogaboam CM, Kunkel SL. Chemokines in the pathogenesis of liver disease: so many players with poorly defined roles. Clin Sci (Lond) 2003;104:47-63.

47. Chien S, Li S, Shiu YT, Li YS. Molecular basis of mechanical modulation of endothelial cell migration. Front Biosci 2005;10:1985-2000.

48. Siefert SA, Sarkar R. Matrix metalloproteinases in vascular physiology and disease. Vascular 2012;20:210-216.

49. Gacche RN, Meshram RJ. Angiogenic factors as potential drug target: efficacy and limitations of anti-angiogenic therapy. Biochim Biophys Acta 2014;1846:161-179.

50. Neufeld G, Kessler O. Pro-angiogenic cytokines and their role in tumor angiogenesis. Cancer Metastasis Rev 2006;25:373-385.

51. Gaudio E, Barbaro B, Alvaro D, Glaser S, Francis H, Ueno Y, Meininger CJ, et al. Vascular endothelial growth factor stimulates rat cholangiocyte proliferation via an autocrine mechanism. Gastroenterology 2006;130:1270-1282.

52. Jimenez-Andrade GY, Ibarra-Sanchez A, Gonzalez D, Lamas M, Gonzalez-Espinosa C. Immunoglobulin E induces VEGF production in mast cells and potentiates their pro-tumorigenic actions through a Fyn kinase-dependent mechanism. J Hematol Oncol 2013;6:56.

53. Kobayashi S, Nakanuma Y, Matsui O. Intrahepatic peribiliary vascular plexus in various hepatobiliary diseases: a histological survey. Hum Pathol 1994;25:940-946.

54. Mancinelli R, Glaser S, Francis H, Carpino G, Franchitto A, Vetuschi A, Sferra R, et al. Ischemia reperfusion of the hepatic artery induces the functional damage of large bile ducts by changes in the expression of angiogenic factors. Am J Physiol Gastrointest Liver Physiol 2015;309:G865-873.

55. Parola M, Marra F, Pinzani M. Myofibroblast - like cells and liver fibrogenesis: Emerging concepts in a rapidly moving scenario. Mol Aspects Med 2008;29:58-66.

56. Imhof BA, Aurrand-Lions M. Angiogenesis and inflammation face off. Nat Med 2006;12:171-172.

57. Trauner M, Meier PJ, Boyer JL. Molecular pathogenesis of cholestasis. N Engl J Med 1998;339:1217-1227.

58. Trauner M, Wagner M, Fickert P, Zollner G. Molecular regulation of hepatobiliary transport systems: clinical implications for understanding and treating cholestasis. J Clin Gastroenterol 2005;39:S111-124.

59. Erlinger S. Physiology of bile flow. Prog Liver Dis 1972;4:63-82.

60. Marin JJ, Macias RI, Briz O, Banales JM, Monte MJ. Bile Acids in Physiology, Pathology and Pharmacology. Curr Drug Metab 2015;17:4-29.

61. Sultan M, Rao A, Elpeleg O, Vaz FM, Abu-Libdeh B, Karpen SJ, Dawson PA. Organic solute transporter-beta (SLC51B) deficiency in two brothers with congenital diarrhea and features of cholestasis. Hepatology 2018;68:590-598.

62. Chen F, Ananthanarayanan M, Emre S, Neimark E, Bull LN, Knisely AS, Strautnieks SS, et al. Progressive familial intrahepatic cholestasis, type 1, is associated with decreased farnesoid X receptor activity. Gastroenterology 2004;126:756-764.

63. Lazaridis KN, LaRusso NF. The Cholangiopathies. Mayo Clin Proc 2015;90:791-800.

64. Alvaro D, Mancino MG. New insights on the molecular and cell biology of human cholangiopathies. Mol Aspects Med 2008;29:50-57.

65. Yoon YB, Hagey LR, Hofmann AF, Gurantz D, Michelotti EL, Steinbach JH. Effect of side-chain shortening on the physiologic properties of bile acids: hepatic transport and effect on biliary secretion of 23-nor-ursodeoxycholate in rodents. Gastroenterology 1986;90:837-852.

66. Alpini G, McGill JM, Larusso NF. The pathobiology of biliary epithelia. Hepatology 2002;35:1256-1268.

67. Floreani A, Mangini C. Primary biliary cholangitis: Old and novel therapy. Eur J Intern Med 2018;47:1-5.

68. Boonstra K, Beuers U, Ponsioen CY. Epidemiology of primary sclerosing cholangitis and primary biliary cirrhosis: a systematic review. J Hepatol 2012;56:1181-1188.

69. Juran BD, Lazaridis KN. Environmental factors in primary biliary cirrhosis. Semin Liver Dis 2014;34:265-272.

70. Hirschfield GM. Diagnosis of primary biliary cirrhosis. Best Pract Res Clin Gastroenterol 2011;25:701-712.

71. Wong LL, Hegade VS, Jones DEJ. What Comes after Ursodeoxycholic Acid in Primary Biliary Cholangitis? Dig Dis 2017;35:359-366.

72. Karlsen TH, Vesterhus M, Boberg KM. Review article: controversies in the management of primary biliary cirrhosis and primary sclerosing cholangitis. Aliment Pharmacol Ther 2014;39:282-301.

73. Eaton JE, Talwalkar JA, Lazaridis KN, Gores GJ, Lindor KD. Pathogenesis of primary sclerosing cholangitis and advances in diagnosis and management. Gastroenterology 2013;145:521-536.

74. Chapman R, Fevery J, Kalloo A, Nagorney DM, Boberg KM, Shneider B, Gores GJ, et al. Diagnosis and management of primary sclerosing cholangitis. Hepatology 2010;51:660-678.

75. Kaplan GG, Laupland KB, Butzner D, Urbanski SJ, Lee SS. The burden of large and small duct primary sclerosing cholangitis in adults and children: a population-based analysis. Am J Gastroenterol 2007;102:1042-1049.

76. Fevery J, Verslype C, Lai G, Aerts R, Van Steenbergen W. Incidence, diagnosis, and therapy of cholangiocarcinoma in patients with primary sclerosing cholangitis. Dig Dis Sci 2007;52:3123-3135.

77. Fosby B, Karlsen TH, Melum E. Recurrence and rejection in liver transplantation for primary sclerosing cholangitis. World J Gastroenterol 2012;18:1-15.

78. Beaven MA. Our perception of the mast cell from Paul Ehrlich to now. Eur J Immunol 2009;39:11-25.

79. Bachelet I, Levi-Schaffer F, Mekori YA. Mast cells: not only in allergy. Immunol Allergy Clin North Am 2006;26:407-425.

80. Bischoff SC, Lorentz A, Schwengberg S, Weier G, Raab R, Manns MP. Mast cells are an important cellular source of tumour necrosis factor alpha in human intestinal tissue. Gut 1999;44:643-652.

81. Cervello M, Foderaa D, Florena AM, Soresi M, Tripodo C, D'Alessandro N, Montalto G. Correlation between expression of cyclooxygenase-2 and the presence of inflammatory cells in human primary hepatocellular carcinoma: possible role in tumor promotion and angiogenesis. World J Gastroenterol 2005;11:4638-4643.

82. Frieri M, Kumar K, Boutin A. Role of mast cells in trauma and neuroinflammation in allergy immunology. Ann Allergy Asthma Immunol 2015;115:172-177.

83. Reber LL, Sibilano R, Mukai K, Galli SJ. Potential effector and immunoregulatory functions of mast cells in mucosal immunity. Mucosal Immunol 2015;8:444-463.

84. da Silva EZ, Jamur MC, Oliver C. Mast cell function: a new vision of an old cell. J Histochem Cytochem 2014;62:698-738.

85. Halova I, Draberova L, Draber P. Mast cell chemotaxis - chemoattractants and signaling pathways. Front Immunol 2012;3:119.

86. Oskeritzian CA, Zhao W, Min HK, Xia HZ, Pozez A, Kiev J, Schwartz LB. Surface CD88 functionally distinguishes the MCTC from the MCT type of human lung mast cell. J Allergy Clin Immunol 2005;115:1162-1168.

87. Schwartz LB. Analysis of MC(T) and MC(TC) mast cells in tissue. Methods Mol Biol 2006;315:53-62.

88. Francis H, Meininger CJ. A review of mast cells and liver disease: What have we learned? Dig Liver Dis 2010;42:529-536.

89. Irani AA, Schechter NM, Craig SS, DeBlois G, Schwartz LB. Two types of human mast cells that have distinct neutral protease compositions. Proc Natl Acad Sci U S A 1986;83:4464-4468.

90. Nakahata T, Kobayashi T, Ishiguro A, Tsuji K, Naganuma K, Ando O, Yagi Y, et al. Extensive proliferation of mature connective-tissue type mast cells in vitro. Nature 1986;324:65-67.

91. Chan A, Cooley MA, Collins AM. Mast cells in the rat liver are phenotypically heterogeneous and exhibit features of immaturity. Immunol Cell Biol 2001;79:35-40.

92. Bradding P, Okayama Y, Howarth PH, Church MK, Holgate ST. Heterogeneity of human mast cells based on cytokine content. J Immunol 1995;155:297-307.

93. Patella V, de Crescenzo G, Ciccarelli A, Marino I, Adt M, Marone G. Human heart mast cells: a definitive case of mast cell heterogeneity. Int Arch Allergy Immunol 1995;106:386-393.

94. Johnson C, Huynh V, Hargrove L, Kennedy L, Graf-Eaton A, Owens J, Trzeciakowski JP, et al. Inhibition of Mast Cell-Derived Histamine Decreases Human Cholangiocarcinoma Growth and Differentiation via c-Kit/Stem Cell Factor-Dependent Signaling. Am J Pathol 2016;186:123-133.

95. Zelechowska P, Agier J, Rozalska S, Wiktorska M, Brzezinska-Blaszczyk E. Leptin stimulates tissue rat mast cell pro-inflammatory activity and migratory response. Inflamm Res 2018;67:789-799.

96. Pincha N, Hajam EY, Badarinath K, Batta SPR, Masudi T, Dey R, Andreasen P, et al. PAI1 mediates fibroblast-mast cell interactions in skin fibrosis. J Clin Invest 2018;128:1807-1819.

97. Chen S, Noordenbos T, Blijdorp I, van Mens L, Ambarus CA, Vogels E, Te Velde A, et al. Histologic evidence that mast cells contribute to local tissue inflammation in peripheral spondyloarthritis by regulating interleukin-17A content. Rheumatology (Oxford) 2018.

98. Elsemuller AK, Tomalla V, Gartner U, Troidl K, Jeratsch S, Graumann J, Baal N, et al. Characterization of mast cell-derived rRNA-containing microvesicles and their inflammatory impact on endothelial cells. FASEB J 2019:fj201801853RR.

99. Xiong L, Zhen S, Yu Q, Gong Z. HCV-E2 inhibits hepatocellular carcinoma metastasis by stimulating mast cells to secrete exosomal shuttle microRNAs. Oncol Lett 2017;14:2141-2146.

100. Jones H, Hargrove L, Kennedy L, Meng F, Graf-Eaton A, Owens J, Alpini G, et al. Inhibition of mast cell-secreted histamine decreases biliary proliferation and fibrosis in primary sclerosing cholangitis Mdr2(-/-) mice. Hepatology 2016;64:1202-1216.

101. Hargrove L, Graf-Eaton A, Kennedy L, Demieville J, Owens J, Hodges K, Ladd B, et al. Isolation and characterization of hepatic mast cells from cholestatic rats. Lab Invest 2016;96:1198-1210.

102. Tsuneyama K, Kono N, Yamashiro M, Kouda W, Sabit A, Sasaki M, Nakanuma Y. Aberrant expression of stem cell factor on biliary epithelial cells and peribiliary infiltration of c-kit-expressing mast cells in hepatolithiasis and primary sclerosing cholangitis: a possible contribution to bile duct fibrosis. J Pathol 1999;189:609-614.

103. Nakamura A, Yamazaki K, Suzuki K, Sato S. Increased portal tract infiltration of mast cells and eosinophils in primary biliary cirrhosis. Am J Gastroenterol 1997;92:2245-2249.

104. Lombardo J, Broadwater D, Collins R, Cebe K, Brady R, Harrison S. Hepatic mast cell concentration directly correlates to stage of fibrosis in NASH. Hum Pathol 2018.

105. Kim DK, Cho YE, Komarow HD, Bandara G, Song BJ, Olivera A, Metcalfe DD. Mastocytosis-derived extracellular vesicles exhibit a mast cell signature, transfer KIT to stellate cells, and promote their activation. Proc Natl Acad Sci U S A 2018;115:E10692-E10701.

106. Eralp A, Menguc NY, Polat E, Yuncu M, Koruk M, Demir SS, Sari I. Preventative Effect of Vitamin E on Mast Cells in Carbon Tetrachlorideinduced Acute Liver Damage. Endocr Metab Immune Disord Drug Targets 2016;16:205-212.

107. Marzioni M, Glaser S, Francis H, Marucci L, Benedetti A, Alvaro D, Taffetani S, et al. Autocrine/paracrine regulation of the growth of the biliary tree by the neuroendocrine hormone serotonin. Gastroenterology 2005;128:121-137.

108. Moncsek A, Al-Suraih MS, Trussoni CE, O'Hara SP, Splinter PL, Zuber C, Patsenker E, et al. Targeting senescent cholangiocytes and activated fibroblasts with B-cell lymphoma-extra large inhibitors ameliorates fibrosis in multidrug resistance 2 gene knockout (Mdr2(-/-)) mice. Hepatology 2018;67:247-259.

109. Graf A, Meng F, Hargrove L, Kennedy L, Han Y, Francis T, Hodges K, et al. Knockout of histidine decarboxylase decreases bile duct ligation-induced biliary

hyperplasia via downregulation of the histidine decarboxylase/VEGF axis through PKA-ERK1/2 signaling. Am J Physiol Gastrointest Liver Physiol 2014;307:G813-823.

110. Meng F, Onori P, Hargrove L, Han Y, Kennedy L, Graf A, Hodges K, et al. Regulation of the histamine/VEGF axis by miR-125b during cholestatic liver injury in mice. Am J Pathol 2014;184:662-673.

111. Popov Y, Patsenker E, Fickert P, Trauner M, Schuppan D. Mdr2 (Abcb4)-/- mice spontaneously develop severe biliary fibrosis via massive dysregulation of pro- and antifibrogenic genes. J Hepatol 2005;43:1045-1054.

112. Ikenaga N, Liu SB, Sverdlov DY, Yoshida S, Nasser I, Ke Q, Kang PM, et al. A new Mdr2(-/-) mouse model of sclerosing cholangitis with rapid fibrosis progression, early-onset portal hypertension, and liver cancer. Am J Pathol 2015;185:325-334.

113. Dale HH, Laidlaw PP. The physiological action of beta-iminazolylethylamine. J Physiol 1910;41:318-344.

114. Branco A, Yoshikawa FSY, Pietrobon AJ, Sato MN. Role of Histamine in Modulating the Immune Response and Inflammation. Mediators Inflamm 2018;2018:9524075.

115. Tanimoto A, Matsuki Y, Tomita T, Sasaguri T, Shimajiri S, Sasaguri Y. Histidine decarboxylase expression in pancreatic endocrine cells and related tumors. Pathol Int 2004;54:408-412.

116. Yatsunami K, Fukui T, Ichikawa A. [Molecular biology of L-histidine decarboxylase]. Yakugaku Zasshi 1994;114:803-822.

117. Medina VA, Brenzoni PG, Lamas DJ, Massari N, Mondillo C, Nunez MA, Pignataro O, et al. Role of histamine H4 receptor in breast cancer cell proliferation. Front Biosci (Elite Ed) 2011;3:1042-1060.

118. Medina VA, Rivera ES. Histamine receptors and cancer pharmacology. Br J Pharmacol 2010;161:755-767.

119. Hocker M, Zhang Z, Koh TJ, Wang TC. The regulation of histidine decarboxylase gene expression. Yale J Biol Med 1996;69:21-33.

120. Meng F, Han Y, Staloch D, Francis T, Stokes A, Francis H. The H4 histamine receptor agonist, clobenpropit, suppresses human cholangiocarcinoma progression by disruption of epithelial mesenchymal transition and tumor metastasis. Hepatology 2011;54:1718-1728.

121. Dickenson JM. Stimulation of protein kinase B and p70 S6 kinase by the histamine H1 receptor in DDT1MF-2 smooth muscle cells. Br J Pharmacol 2002;135:1967-1976.

122. Mitsuhashi M, Mitsuhashi T, Payan DG. Multiple signaling pathways of histamine H2 receptors. Identification of an H2 receptor-dependent Ca2+ mobilization pathway in human HL-60 promyelocytic leukemia cells. J Biol Chem 1989;264:18356-18362.

123. Lovenberg TW, Roland BL, Wilson SJ, Jiang X, Pyati J, Huvar A, Jackson MR, et al. Cloning and functional expression of the human histamine H3 receptor. Mol Pharmacol 1999;55:1101-1107.

124. Liu C, Ma X, Jiang X, Wilson SJ, Hofstra CL, Blevitt J, Pyati J, et al. Cloning and pharmacological characterization of a fourth histamine receptor (H(4)) expressed in bone marrow. Mol Pharmacol 2001;59:420-426.

125. Melillo RM, Guarino V, Avilla E, Galdiero MR, Liotti F, Prevete N, Rossi FW, et al. Mast cells have a protumorigenic role in human thyroid cancer. Oncogene 2010;29:6203-6215.

126. Osawa Y, Seki E, Adachi M, Suetsugu A, Ito H, Moriwaki H, Seishima M, et al. Role of acid sphingomyelinase of Kupffer cells in cholestatic liver injury in mice. Hepatology 2010;51:237-245.

127. Niranjan R, Mavi P, Rayapudi M, Dynda S, Mishra A. Pathogenic role of mast cells in experimental eosinophilic esophagitis. Am J Physiol Gastrointest Liver Physiol 2013;304:G1087-1094.

128. Kumar D, Pandya SK, Varshney S, Shankar K, Rajan S, Srivastava A, Gupta A, et al. Temporal immmunometabolic profiling of adipose tissue in HFD-induced obesity: manifestations of mast cells in fibrosis and senescence. Int J Obes (Lond) 2018.

129. Xu N, An J. Formononetin ameliorates mast cell-mediated allergic inflammation via inhibition of histamine release and production of pro-inflammatory cytokines. Exp Ther Med 2017;14:6201-6206.

130. Wang Y, Aoki H, Yang J, Peng K, Liu R, Li X, Qiang X, et al. The role of sphingosine 1-phosphate receptor 2 in bile-acid-induced cholangiocyte proliferation and cholestasis-induced liver injury in mice. Hepatology 2017;65:2005-2018.

131. Patsenker E, Popov Y, Stickel F, Jonczyk A, Goodman SL, Schuppan D. Inhibition of integrin alphavbeta6 on cholangiocytes blocks transforming growth factor-beta activation and retards biliary fibrosis progression. Gastroenterology 2008;135:660-670.

132. Ueno Y, Fukushima K, Nakagome Y, Kido O, Shimosegawa T. Bioinformatic approach for cholangiocyte pathophysiology. Hepatol Res 2007;37 Suppl 3:S444-448.

133. Nakamura Y, Franchi L, Kambe N, Meng G, Strober W, Nunez G. Critical role for mast cells in interleukin-1beta-driven skin inflammation associated with an activating mutation in the nlrp3 protein. Immunity 2012;37:85-95.

134. Kruger-Krasagakes S, Moller A, Kolde G, Lippert U, Weber M, Henz BM. Production of interleukin-6 by human mast cells and basophilic cells. J Invest Dermatol 1996;106:75-79.

135. Guicciardi ME, Krishnan A, Bronk SF, Hirsova P, Griffith TS, Gores GJ. Biliary tract instillation of a SMAC mimetic induces TRAIL-dependent acute sclerosing cholangitis-like injury in mice. Cell Death Dis 2017;8:e2535.

136. Miyazawa S, Hotta O, Doi N, Natori Y, Nishikawa K, Natori Y. Role of mast cells in the development of renal fibrosis: use of mast cell-deficient rats. Kidney Int 2004;65:2228-2237.

137. Kong P, Christia P, Frangogiannis NG. The pathogenesis of cardiac fibrosis. Cell Mol Life Sci 2014;71:549-574.

138. Sugihara A, Tsujimura T, Fujita Y, Nakata Y, Terada N. Evaluation of role of mast cells in the development of liver fibrosis using mast cell-deficient rats and mice. J Hepatol 1999;30:859-867.

139. Veerappan A, O'Connor NJ, Brazin J, Reid AC, Jung A, McGee D, Summers B, et al. Mast cells: a pivotal role in pulmonary fibrosis. DNA Cell Biol 2013;32:206-218.

140. Shao Z, Nazari M, Guo L, Li SH, Sun J, Liu SM, Yuan HP, et al. The cardiac repair benefits of inflammation do not persist: evidence from mast cell implantation. J Cell Mol Med 2015;19:2751-2762.

141. Francis H, DeMorrow S, Venter J, Onori P, White M, Gaudio E, Francis T, et al. Inhibition of histidine decarboxylase ablates the autocrine tumorigenic effects of histamine in human cholangiocarcinoma. Gut 2012;61:753-764.

142. Garcia-Roman J, Ibarra-Sanchez A, Lamas M, Gonzalez Espinosa C. VEGF secretion during hypoxia depends on free radicals-induced Fyn kinase activity in mast cells. Biochem Biophys Res Commun 2010;401:262-267.

143. Ghosh AK, Hirasawa N, Ohtsu H, Watanabe T, Ohuchi K. Defective angiogenesis in the inflammatory granulation tissue in histidine decarboxylase-deficient mice but not in mast cell-deficient mice. J Exp Med 2002;195:973-982.

144. Washington K, Clavien PA, Killenberg P. Peribiliary vascular plexus in primary sclerosing cholangitis and primary biliary cirrhosis. Hum Pathol 1997;28:791-795.

145. Lilla JN, Werb Z. Mast cells contribute to the stromal microenvironment in mammary gland branching morphogenesis. Dev Biol 2010;337:124-133.

146. Chen J, Chen L, Zern MA, Theise ND, Diehl AM, Liu P, Duan Y. The diversity and plasticity of adult hepatic progenitor cells and their niche. Liver Int 2017;37:1260-1271.

147. Wang Q, Zhao DY, Xu H, Zhou H, Yang QY, Liu F, Zhou GP. Down-regulation of microRNA-223 promotes degranulation via the PI3K/Akt pathway by targeting IGF-1R in mast cells. PLoS One 2015;10:e0123575.

148. Azizollahi HR, Rafeey M. Efficacy of proton pump inhibitors and H2 blocker in the treatment of symptomatic gastroesophageal reflux disease in infants. Korean J Pediatr 2016;59:226-230.

149. Ahmadi A, Ebrahimzadeh MA, Ahmad-Ashrafi S, Karami M, Mahdavi MR, Saravi SS. Hepatoprotective, antinociceptive and antioxidant activities of cimetidine, ranitidine and famotidine as histamine H2 receptor antagonists. Fundam Clin Pharmacol 2011;25:72-79.